CHAPTER - 5

RESULTS AND DISCUSSION

This chapter discusses the results and discussion of different perovskite catalysts which were characterized by various techniques such as SEM, XRD, BET surface area, FTIR, XPS, and TEM etc as well as the catalytic activities of the catalysts were studied for the simultaneous removal of NO and soot combustion. Activities of the catalyst were correlated with their physico-chemical characteristics.

5.1 Effects of Calcination Temperature of $LaFeO_3$

The $LaFeO_3$ catalyst was prepared by sol-gel method was examined at different calcinations temperature such as 600, 650, 700, and 750°C in stagnant air for 6h to confirm the best calcination temperature, as shown in Table 5.1. The temperature at 700°C was found to be the best calcination temperature for the simultaneous removal of soot and NO.

Table 5.1 Optimization of calcination temperature of $LaFeO_3$

S. No.	Catalyst Composition	Name of Catalyst	Preparation Method	Calcination strategies
Optimization of calcination temp				
1.	$LaFeO_3$	LFes600	Sol-gel	600°C, 6h, Air
2.	$LaFeO_3$	LFes650	Sol-gel	650°C, 6h, Air
3.	**$LaFeO_3$**	**LFes700**	**Sol-gel**	**700°C, 6h, Air**
4.	$LaFeO_3$	LFes750	Sol-gel	750°C, 6h, Air

5.1.1 Structural and morphological characterization of catalysts

5.1.1.1 Scanning electron microscope (SEM) characterization results

The SEM images of $LaFeO_3$ prepared by sol-gel methods and optimizing with temperatures with 600, 650, 700, and 750°C. The SEM micrographs at 10 KX

magnifications shown in Figure 5.1 revealed that the prepared catalyst samples were highly porous and aggregated. The morphologies of particles are irregular shape; granular particles were within the nanoscale 40 and 100 nm calculated by "Image J software" with varying degree of agglomeration. In the comparison of optimization temperature of $LaFeO_3$, the calcination temperature at 700°C (LFes700) was more uniform and the porous surface can be visualized (Figure 5.1 B).

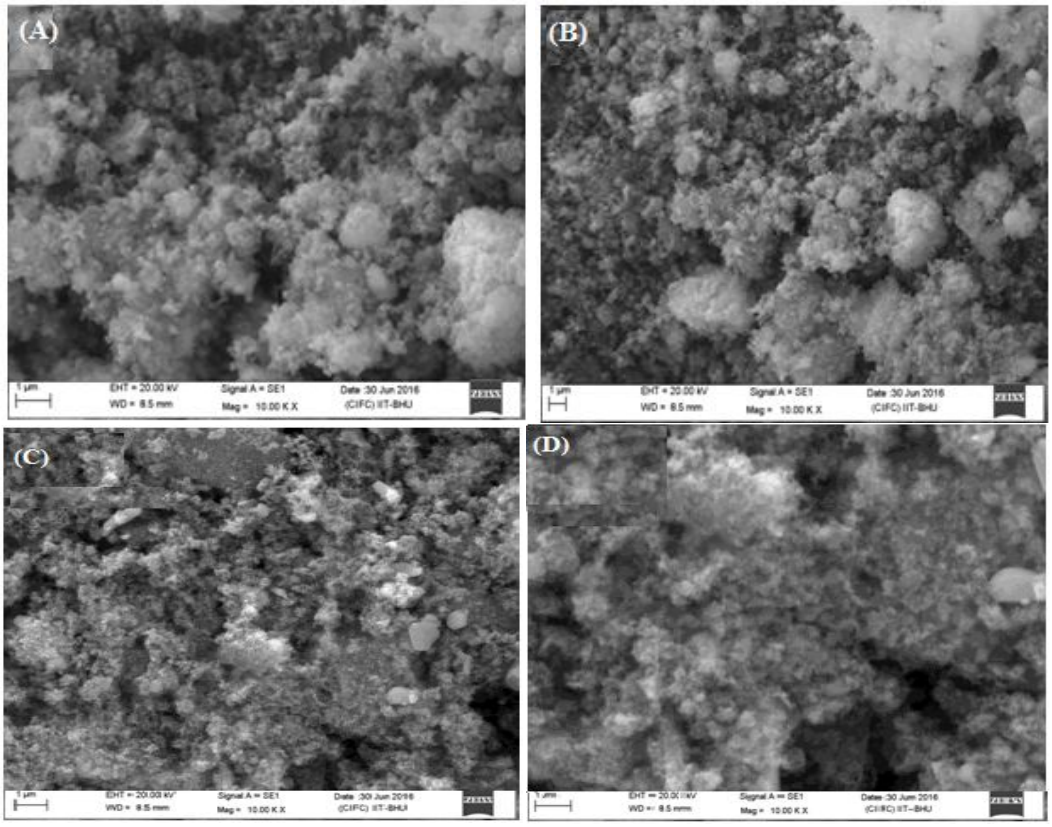

Figure 5.1 Scanning electron micrographs of LFes600 (A), (B) LFes650 (C) LFes700, (D) LFes750

The LFes700 catalyst calcined at 700°C has highest surface area as compared to catalyst calcined at different temperature. The pore volume also follows the same trend. The average pore diameter of LFes700°C is smallest following the order: LFes700 > LFes750 > LFes650 > LFes700.

Table 5.2 Effect of calcination temperature on textural properties of $LaFeO_3$ perovskite catalyst

Catalyst sample	Surface area (m^2/g)	Pore volume (cm^3/g)	Average pore dia. (nm)	Crystallite size (nm)
LFes600	8.98	0.0044	38.79	56.33
LFes650	14.87	0.0052	36.34	52.87
LFes700	**16.53**	**0.0058**	**32.80**	**44.28**
LFes750	15.45	0.0056	34.93	51.67

5.1.1.2 Energy dispersive X-ray (EDX)

It was evident from the results of EDX analysis that all catalysts are pure due to the presence of only La, Fe, and O. There are no other elements present in the spectra as shown Figure 5.2 and Table 5.3. EDX results are also the good harmony with XRD results. The results of EDX are closer with the composition taken during the preparation of the catalysts.

Table 5.3 Atomic % data of LFes700

S.L.	Element	Weight%	Atomic%
1	O K	58.68	65.51
2	Fe K	10.82	13.74
4	La K	30.91	20.75
Totals		100.00	100

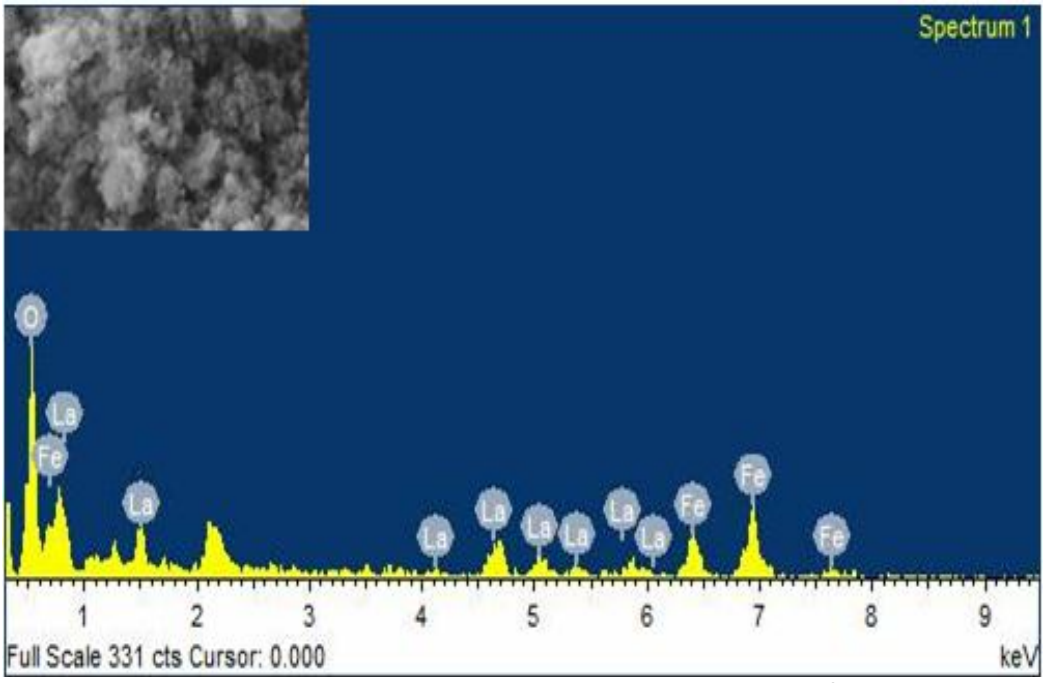

Figure 5.2 Energy dispersive X-ray spectra catalyst of LFes700

5.1.1.3 XRD analysis

X-ray diffraction (XRD) studies of the catalysts were carried out to identify the phase and structure of the catalysts. XRD patterns of perovskite catalysts prepared by sol-gel method and calcinations with different temperature 600, 650, 700, and 750°C. The detailed X-Ray diffraction patterns are shown in Figure 5.3. The 2-theta values for $LaFeO_3$ show that the catalyst has rhombohedral perovskite phase (JCPDS 89-8775). The XRD location peak in XRD patterns of LFes600, LFes650, LFes700, and LFes750 are almost same. Knowing the width of XRD peak and Scherrer equation, the calculated nano-crystalline is presented in Table 5.2.

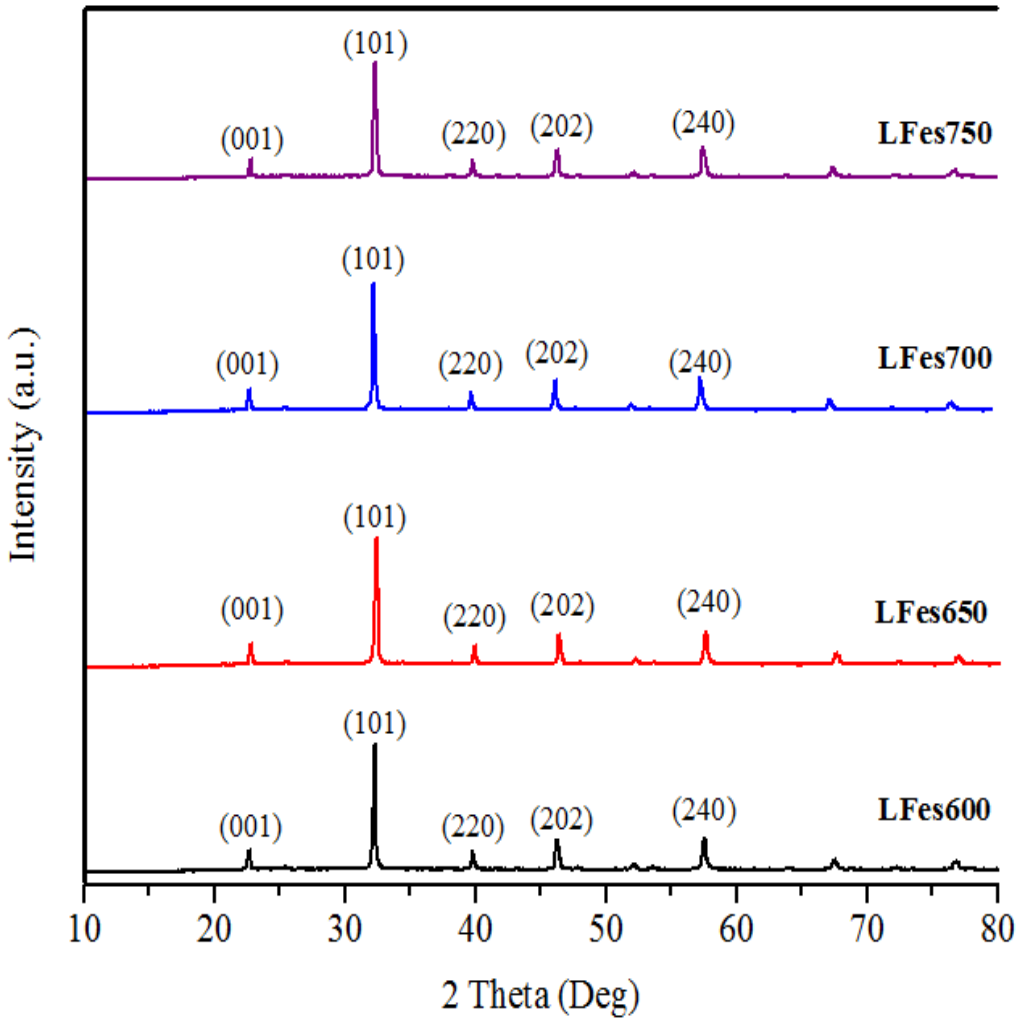

Figure 5.3 XRD of $LFeO_3$ at different calcination temp of 600, 650, 700, 750°C

5.1.1.4 FTIR Characterization

Figure 5.4 depicts the infrared absorption spectra of the $LaFeO_3$ catalyst prepared by sol-gel method and calcined at 700°C. The broad absorption bands around 3402 cm^{-1} appeared in the IR spectra of the as-prepared $LaFeO_3$ corresponded to OH stretching and OH bending of water. The absorption band at 559 cm^{-1} related to Fe-O stretching vibration, which was confirmed with the reported value that iron-oxygen stretching appears at around 600 cm^{-1} [Khalil 2003].

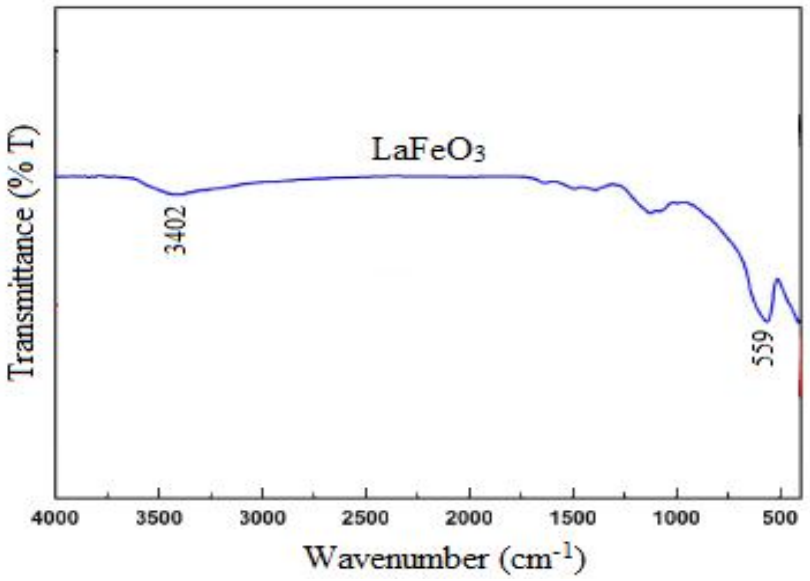

Figure 5.4 FTIR spectra of the LFes700 catalyst

5.1.1.5 XPS analysis of the catalysts

The characteristic spectra collected for La3d, Fe2p and O1s in $LaFeO_3$ perovskite of calcinations 700°C are displayed in Figures 5.5-5.7 respectively. On the basis of the binding energies of the Fe2p main lines, as shown in Figure 5.6, it is difficult to determine the oxidation states of iron cations because similar values can be obtained for most of the iron oxides and hydroxides.

The XPS La 3d and Fe 2p core-level spectra revealed that the lanthanum and iron atoms were in the formal chemical valance state of +3 in the $LaFeO_3$. The high-resolution spectrum of La3d (Figure 5.5) showed two strong La peaks at 835.8 and 852.9 eV corresponding to spin-orbit splitting of $3d_{5/2}$ and $3d_{3/2}$ of La^{3+} ions in oxide form. The binding energies of Fe $2p_{3/2}$ and $Fe2p_{1/2}$ were observed at 711.1 and 723.8 eV (Figure 5.6), which corresponded to the core level spectra of Fe^{3+} ions in their oxide form.

The high-resolution spectrum of O 1s could be deconvolved into two peaks by Gaussian rule. The two peaks were wide and asymmetric, indicating that there were at least two kinds of O chemical states. The major one corresponding to the binding energy at 531.8 eV was assigned to chemically absorbed hydroxyl oxygen species, while the shoulder one at 529.4 eV was attributed to the lattice oxygen species. It could be concluded that there was abundant hydroxyl oxygen on the catalyst, which was an important parameter to influence the catalytic performances in the oxidation reaction.

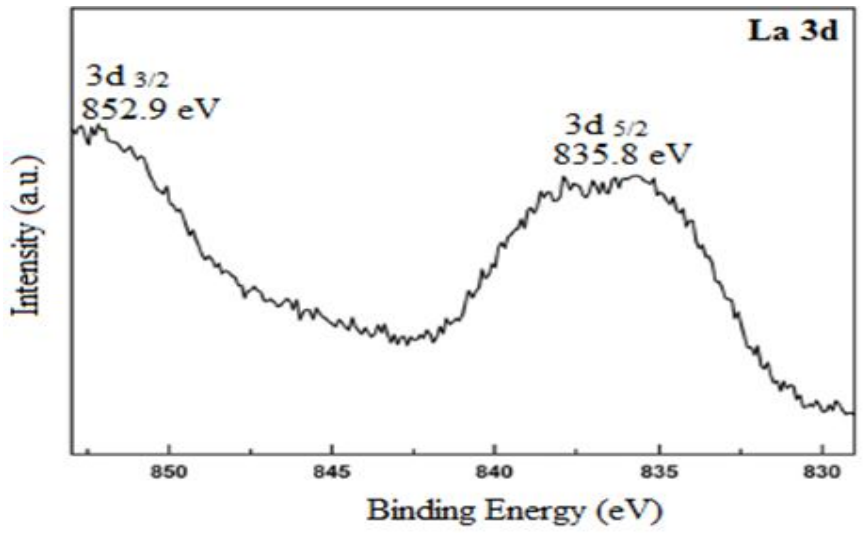

Figure 5.5 Interface characteristics of the sample La 3d

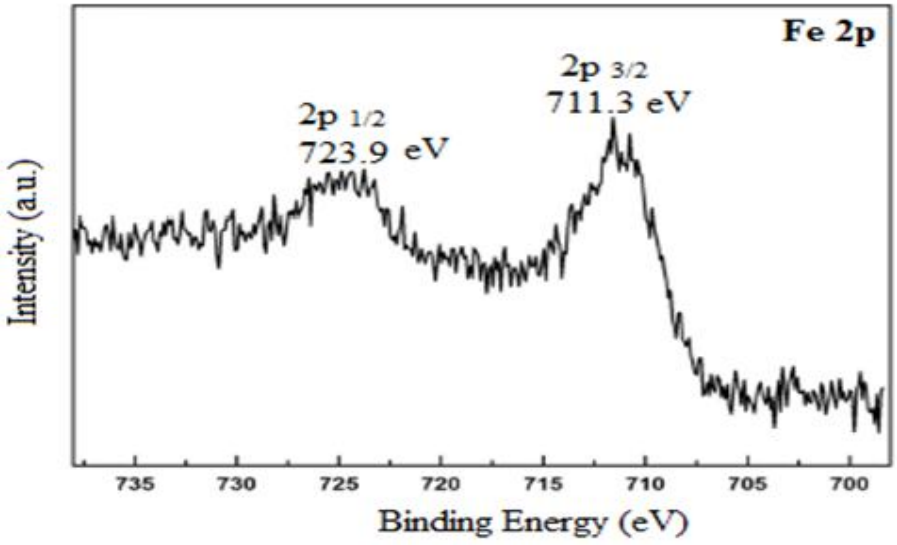

Figure 5.6 Interface characteristics of the sample Fe 2p

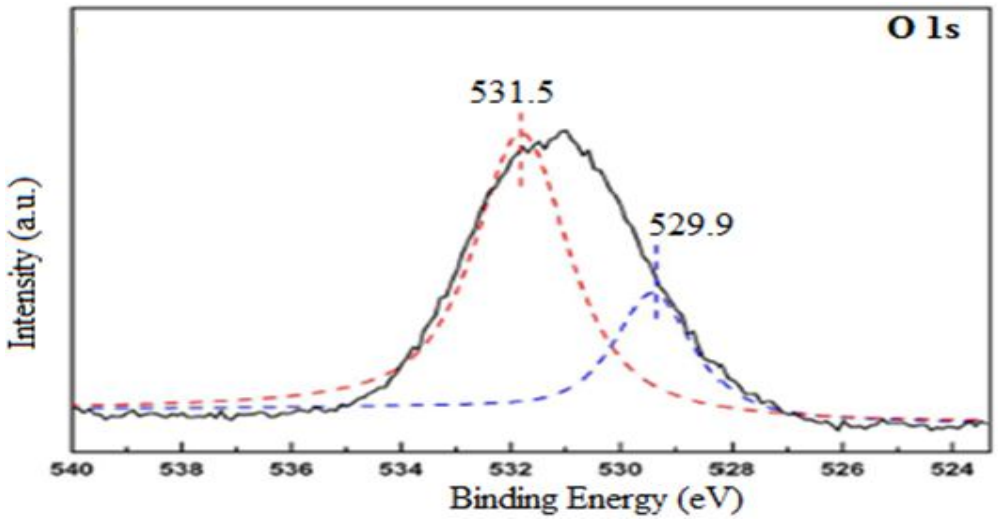

Figure 5.7 Interface characteristics of the sample O 1s

5.1.2 Catalysts activity tests for simultaneous combustion of soot and reduction NO

5.1.2.1 Soot combustion

The catalytic combustion tests of diesel soot were performed over the catalyst samples prepared by the sol-gel method as a function of temperature. The reproducibility of the experimental data was confirmed by repeating some of the tests for at least thrice. Activity of the catalyst for soot oxidation was evaluated on the basis of light off temperature characteristics T_i, T_{10}, T_{50} and T_f where, T_i, T_{10}, T_{50}, and T_f are temperatures corresponding to the start of soot ignition, 10% conversion of soot, 50% conversion of soot and total oxidation of soot respectively. Experiments for simultaneous reduction of soot and NOx were planned to run from 0°C to700^{o}C at a 10°C min^{-1} rate. The catalytic activity of the prepared catalysts was tested in a Bench Scale Reactor System. The Standard gas mixtures are as follows: NO-Ar mixture flow rate = 30 mL/min, Oxygen flow rate = 10 mL/min, Ar balance, Total flow rate = 100 mL/min via a set of mass flow meters (Brooks) to a fixed-bed microreactor enclosed in a quartz tube placed in an electric oven. The tubular quartz reactor was loaded with 110 mg of a 1:10 by weight mixture of soot and powdered catalyst (tight contact).

The first series of experiments were conducted to see the calcinations effect of $LaFeO_3$ perovskite catalyst for simultaneous removal of soot and NO. Four catalysts LFes600, LFes650, LFes700, and LFes750 were tested for soot oxidation. It can be seen from the Figure 5.8 that the (10%) oxidation of diesel soot over different catalyst LFes600, LFes650, LFes700, LFes750 initiated at different temperatures of 217, 196, 168, and 181°C respectively. Similarly, the temperatures for total oxidation of the soot over different catalyst LFes600, LFes650, LFes700, and LFes750 were 482, 514, 429, and 436°C respectively. All catalysts showed total combustion of the soot at temperature < 500°C, i.e. within the temperature window of diesel exhaust. It is can be concluded from the results reported in the Figure 5.8 and Table 5.4 that LFes700 catalyst is the best for soot oxidation under the present experimental conditions. The catalytic activity of the catalyst samples chiefly depends on three factors: chemical composition, the degree of crystallinity, and the crystals morphology (including particle sizes, pore size distribution, and specific surface area of the perovskite catalyst).

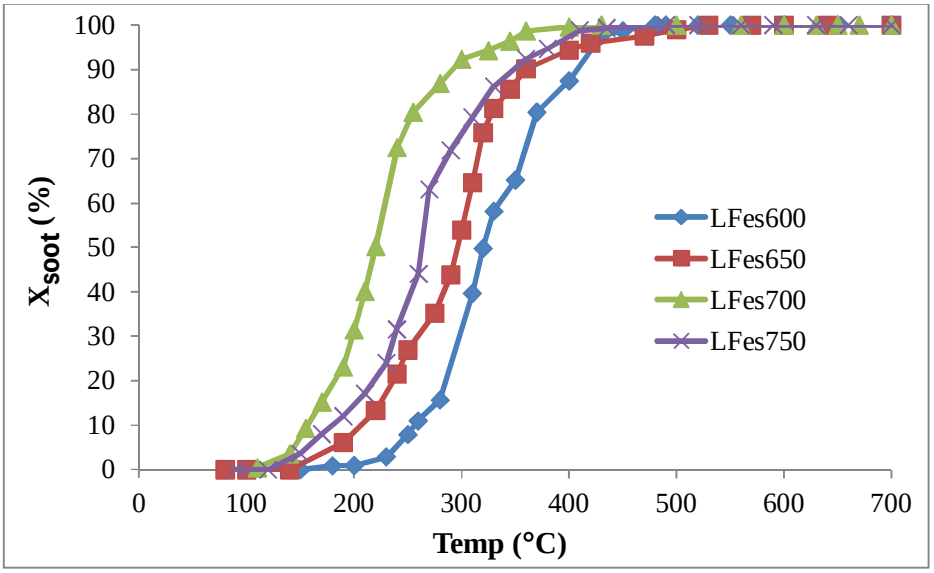

Figure 5.8 Soot conversions of $LFeO_3$ at different calcinations temp of 600, 650, 700, and 750°C

Table 5.4 Soot conversion of $LaFeO_3$ at different calcinations Temperature

S. N.	Catalyst	Soot oxidation			
		T_{10} (°C)	T_{50} (°C)	T_{100} (°C)	T_p (°C)
1.	LFes600	217	322	482	441
2.	LFes650	196	290	514	365
3.	**LFes700**	168	218	429	323
4.	LFes750	181	267	436	422

5.1.2.2 NO reduction

The experimental study conducted for LFes600, LFes650, LFes700, and LFes750 catalyst. In Figure 5.9 and Table 5.5 compared NO conversions of cata-LFes600 obtained by the sol-gel method and calcined with different temperature strategies (600, 650, 700, and 750°C) under steady-state reaction conditions as a function of the reaction temperature. The LFes700 catalyst has better NO conversion activity than all above prepared catalyst. The catalyst is showed maximum 54% conversion of NO at 325°C. Therefore based on the experiments calcinations temperature at 700°C was found to be the optimum temperature for LaFes series catalyst.

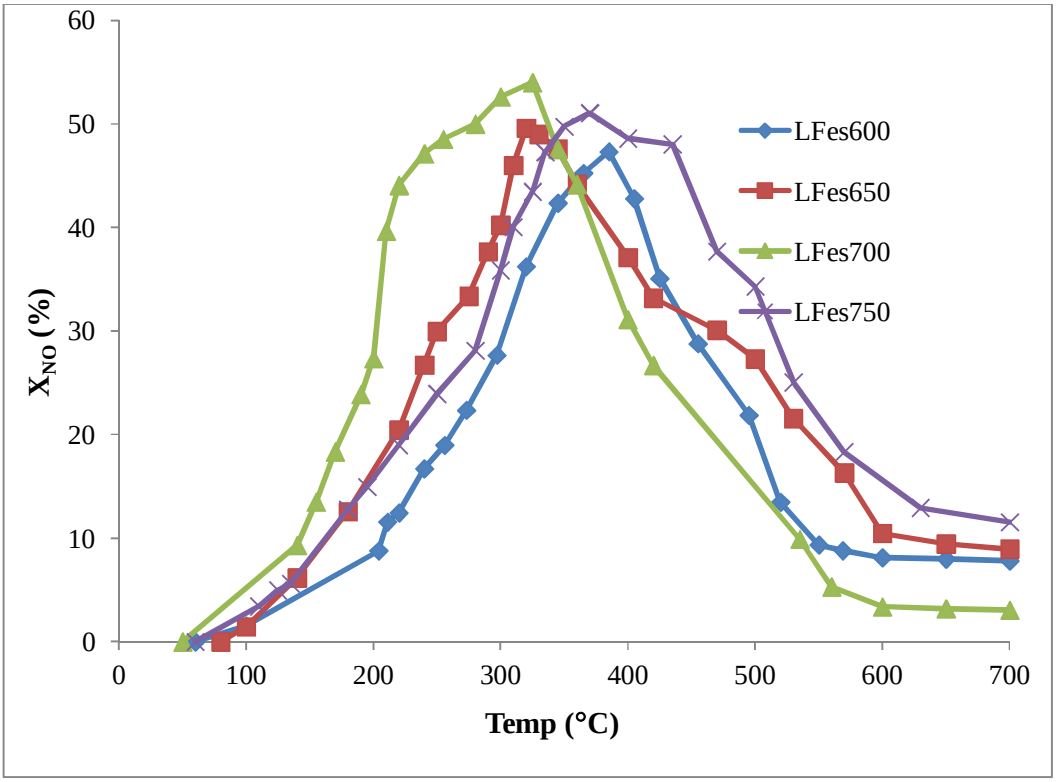

Figure 5.9 NO conversion of $LFeO_3$ at different calcinations temp of 600, 650, 700, 750°C

Table 5.5 NO conversion of $LaFeO_3$ at different calcinations Temperature

S. N.	Catalyst	NO reduction	
		T_{max} (°C)	X_{NO} (%)
1.	LFes600	384	47.31
2.	LFes650	319	49
3.	**LFes700**	**325**	**54**
4.	LFes750	372	51.05

5.2 Effect of preparation methods of $LaFeO_3$

Methods of catalyst preparations are also an important aspect in order to synthesize the highly active catalyst. Sol-gel, reactive grinding, and solution combustion methods of preparation have been used in the present study to compare the activities of the prepared catalysts for simultaneous removal soot and NO.

5.2.1 Structural and morphological characterization of catalysts

5.2.1.1 Scanning electron microscope (SEM) characterization results

The SEM images of $LaFeO_3$ prepared by solution combustion synthesis (SCS) and reactive grinding methods were compared with the sol-gel method, all the precursors calcined at 700°C. The SEM micrographs at 10 KX magnifications shown in Figure 5.10 revealed that the catalyst prepared by SCS and RG were porous. The morphologies of particles are irregular shape; granular particles were also between 40 and 100 nm calculated by "Image J software" with more agglomeration as compared to the sample prepared by sol-gel method. In comparison to the above methods, the sol-gel method of preparation was found to be the best with highly porous and uniform surface.

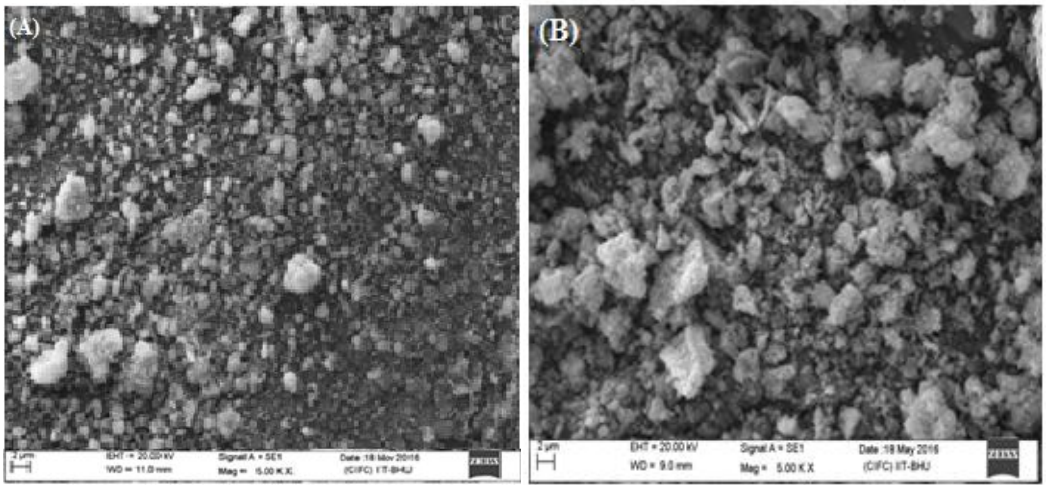

Figure 5.10 Scanning electron micrographs of (A) LFesc700 and (B) LFerg700

Textural characterization of the catalysts

Typical nitrogen physisorption isotherms and pore size distribution curves for the catalyst samples prepared by three different methods and calcined at 700°C are shown in Figure 5.10 (A) and (B) respectively. The nitrogen sorption isotherms exhibit type-IV isotherms with H1 type hysteresis loop. This type of isotherm occurs on porous adsorbent with pores in the range of 1.5-100 nm as can be visualized on pore size

distributions curves in Figure 5.11. The narrow area of the hysteresis loop present in the sorption isotherms of all the samples is a representative of open-textured pores, which offers practically negligible diffusion resistance during the reaction. The pore size distributions of the catalysts LFes700, LFesc700 and LFerg700 are shown in Figure 5.12 a, b and c respectively. It can be seen that the pore size distribution is curves for LFes700, LFesc700, and LFerg700 are similar in nature. In the case of LFes700, the pore size distribution is bimodal having the most probable pore found around 340 Å with a distinct second peak at around 95 Å, while in the case of LFerg700 the first peak appeared around 98 Å with another one around 350 Å. In case of LFesc700, the most probable pore was found near 340 Å which is wider in comparison to other two catalysts.

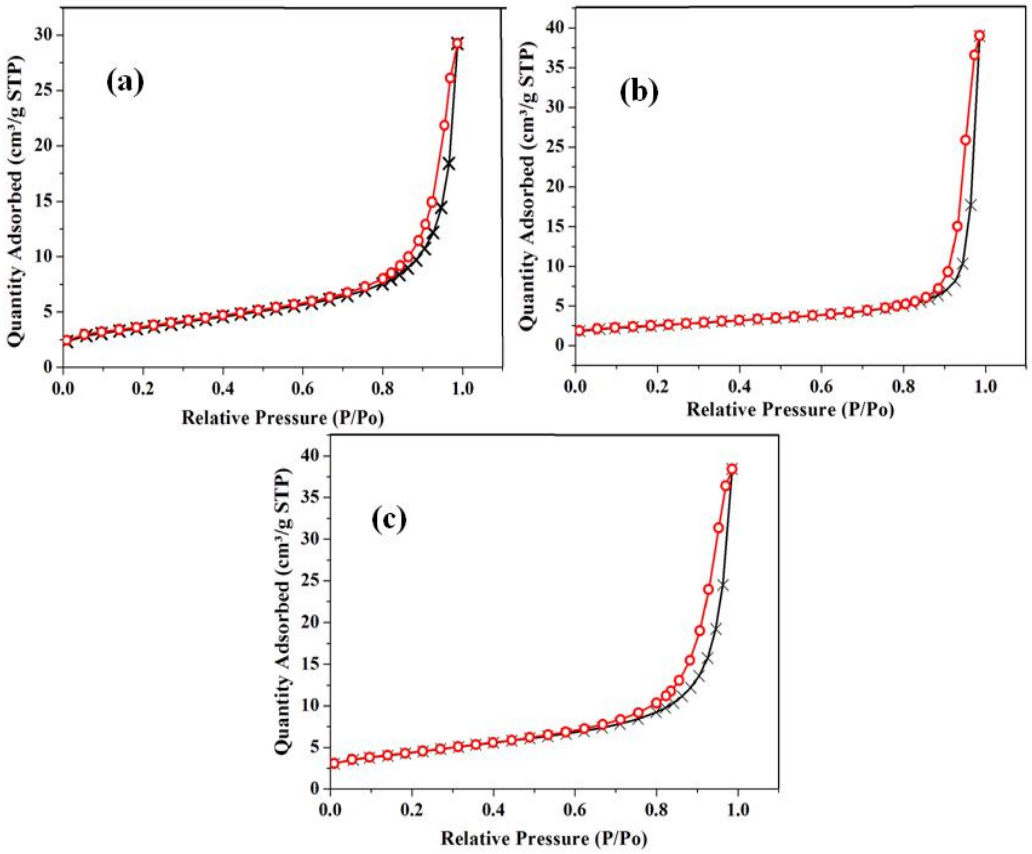

Figure 5.11 N_2 Physisorption isotherms of catalysts (a) LFes700 (b) LFesc700 and (c) LFerg700 calcined at 700°C

The average pore diameter obtained by BET analysis suggests that catalyst was mesoporous. The initial part of the isotherm is attributed to monolayer adsorption. At higher pressures the slope shows increased uptake of adsorbate as the pores become filled, inflection point typically occurs near the completion of the first monolayer. In the mesoporous materials, due to larger pores, the greater number of molecules interacts with each other and displays better catalytic activity. Hysteresis loops occur at moderate relative pressures (around 0.8) and the area within the loop is very small suggesting open cylindrical pores of the catalyst.

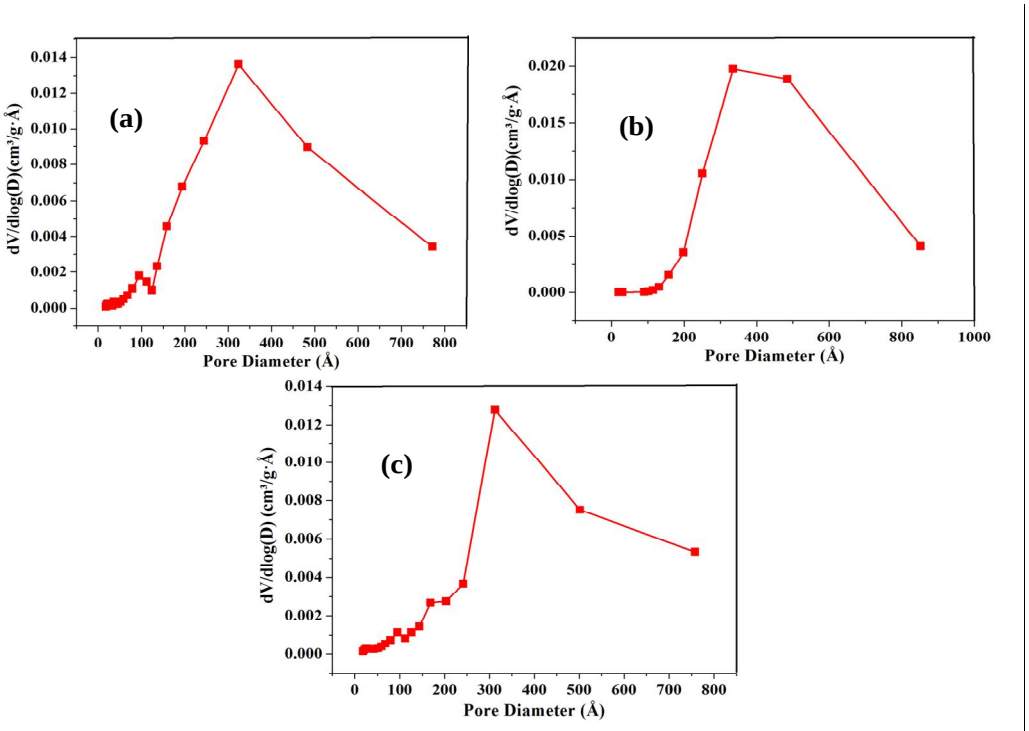

Figure 5.12 Pore size distribution curves of catalysts (a) LFes700 (b) LKFes700 and (c) LKFeCus700-B

The textural properties determined by low-temperature N_2 physisorption, including BET surface area; total pore volume and average pore diameter of the perovskites studied in the present investigation are summarized in Table 5.6. It can be seen that the various perovskite have a low specific surface area (7-15m^2/g) and Average pore size (13-20 Å), which is in expected range considering the high synthesis

temperature. This is in accordance with references [Russo *et al*., 2008, Campagnoli *et al*., 2005]. The catalysts formed at 700^{o}C showed the highest surface area irrespective of the preparation methods. Similarly, the catalyst obtained at 650°C displayed the lowest surface area irrespective of the preparation methods. It is very interesting to note that the catalyst (LFes700) prepared by sol-gel and calcined at 700^{o}C exhibited the highest surface area (16.53 m^2/g), the lowest pore volume (0.0058 cm^3/g) and comparable average pore size as compared to catalysts prepared by other methods and calcined at the same temperature.

Table 5.6 Textural characterization of perovskite catalyst samples

Catalyst sample	Surface area (m^2/g)	Pore volume (cm^3/g)	Average pore dia. (nm)	Crystallite size (nm)
LFes700	**16.53**	**0.0058**	**32.80**	**44.28**
LFesc700	09.12	0.0074	40.32	54.01
LFerg700	12.02	0.0049	41.56	45.33
LCos700	13.39	0.0543	43.38	48.67
LMns700	11.45	0.0040	44.07	61.34

5.2.1.2 XRD analysis

X-ray diffraction (XRD) studies of the catalysts were carried out to identify the phase and structure of the catalysts. XRD patterns of $LaFeO_3$ catalysts prepared by sol-gel method, SCS, and RG method and calcinations with temperature 700°C. The detailed X-Ray diffraction patterns are shown in Figure 5.13. The 2-theta values for $LaFeO_3$ show that the catalyst has rhombohedral perovskite phase (JCPDS 89-8775). The XRD location peak in XRD patterns of LFesc700 and LFerg700 are almost same and LFes700 catalyst showing sharp peak comparing with above catalysts. Knowing the width of XRD peak and Scherrer equation, the calculated nano-crystalline is presented in Table 5.6.

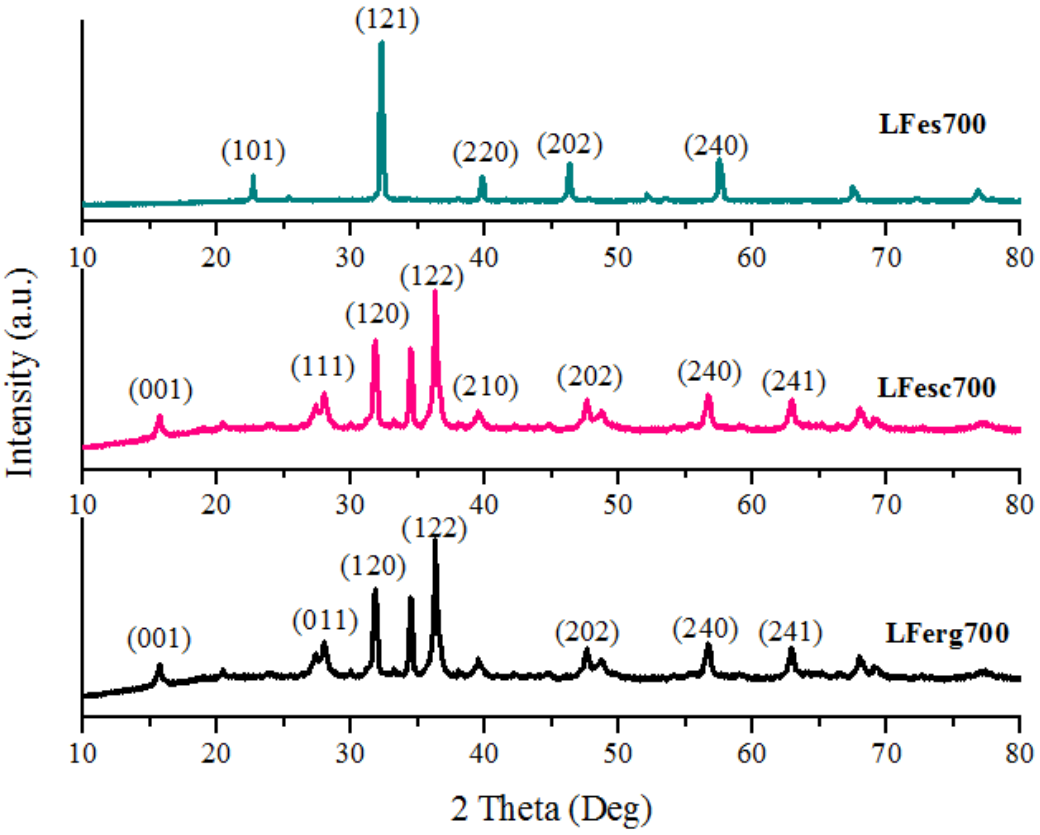

Figure 5.13 XRD of $LFeO_3$ at different preparations method 700°C

5.2.2 Catalysts activity tests for simultaneous combustion of soot and reduction NO

5.2.2.1 Soot combustion

After confirming the calcination temperature, further the $LaFeO_3$ catalyst was prepared by the solution combustion synthesis method (LaFesc700), reactive grinding method (LaFerg700) and sol-gel method (LaFes700) and their activity simultaneous soot and NO removal were compared as shown in Figure 5.14 and Table 5.7. In case of SCS the total soot oxidation was found at 451°C, while in case of RG method it occurred at 15°C higher temperature while the total soot combustion took place at much lower temperature of 429°C in case of SG method. The crystallite size of the LaFes700 showed smallest size. Thus, the specific activity increases when the degree of crystallization decreases. Therefore, catalyst prepared by sol-gel method gives best activity for soot oxidation.

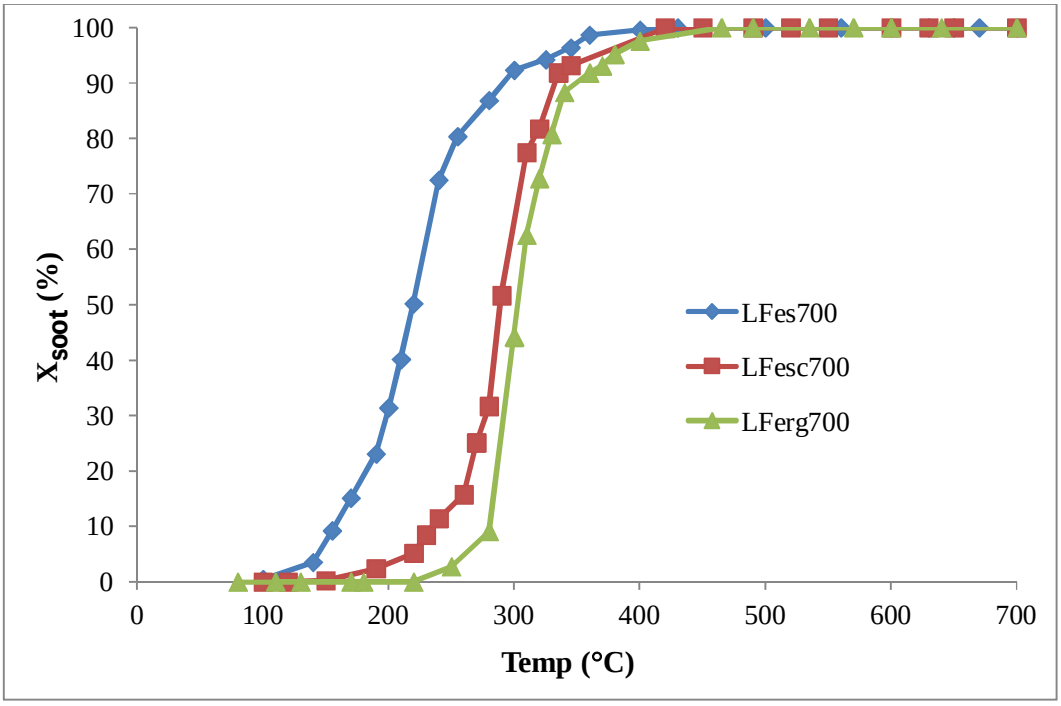

Figure 5.14 Comparison of soot conversion activity of $LaFeO_3$ catalyst by different preparation method

Table 5.7 Effect of preparation method of $LaFeO_3$ catalyst

S. L.	Catalyst	Soot oxidation				NO reduction	
		T_{10} (°C)	T_{50} (°C)	T_{100} (°C)	T_p (°C)	T_{max} (°C)	X_{NO} (%)
1	**LFes700**	**168**	**218**	**429**	**323**	**325**	**54**
2	LFesc700	236	283	451	344	335	46.91
3	LFerg700	288	301	466	361	342	43.45

5.2.2.2 NO reduction

After confirming the calcination temperature, further the $LaFeO_3$ catalyst was prepared by the solution combustion synthesis method (LaFesc700), reactive grinding method (LaFerg700) and sol-gel method (LaFes700) and their activity simultaneous soot and NO removal were compared. In case of SCS the maximum NO reduction of 46.91% was found at 335°C, while in case of RG method it occurred at 342°C for

43.45% NO reduction while maximum of 54% reduction took place at much lower temperature of 325°C in case of SG method. Therefore, catalyst prepared by sol-gel method gives best activity for NO reduction as shown in Figure 5.15.

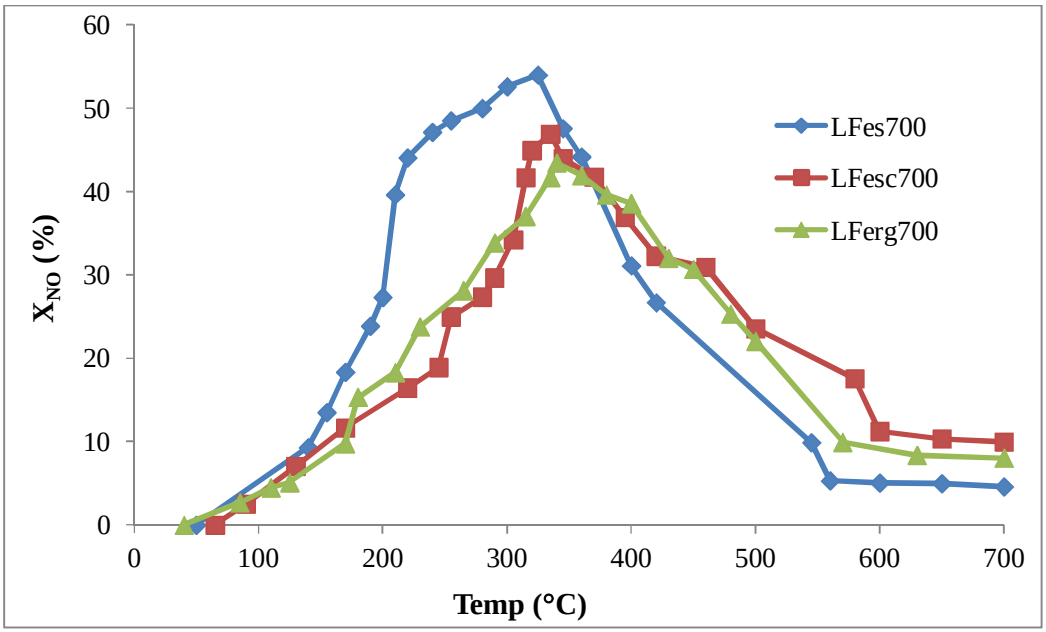

Figure 5.15 Comparison of NO conversion activity of $LaFeO_3$ catalyst by different preparation method

5.3 Screening of the catalysts using above optimization parameters.

On the basis of above experiments, upon optimization it was found that perovskite catalyst prepared by sol-gel method followed by calcinations at 700°C gives best activity for simultaneous removal of soot and NO. Further, activity of LFes700 was compared with lathnum cobalt (LaCos700) and lanthanum manganese (LaMns700) perovskite catalysts.

5.3.1 Structural and morphological characterization of catalysts

5.3.1.1 Scanning electron microscope (SEM) characterization results

The SEM images of LCos700 and LMns700 catalyst. The SEM micrographs at 5KX magnifications shown in Figure 5.16 revealed that the prepared catalyst samples were comparably lower porous and aggregated than the LFes700. The morphologies of

particles are irregular shape; granular particles were within the nanoscale 40 and 100 nm calculated by “Image J software” with varying degree of agglomeration.

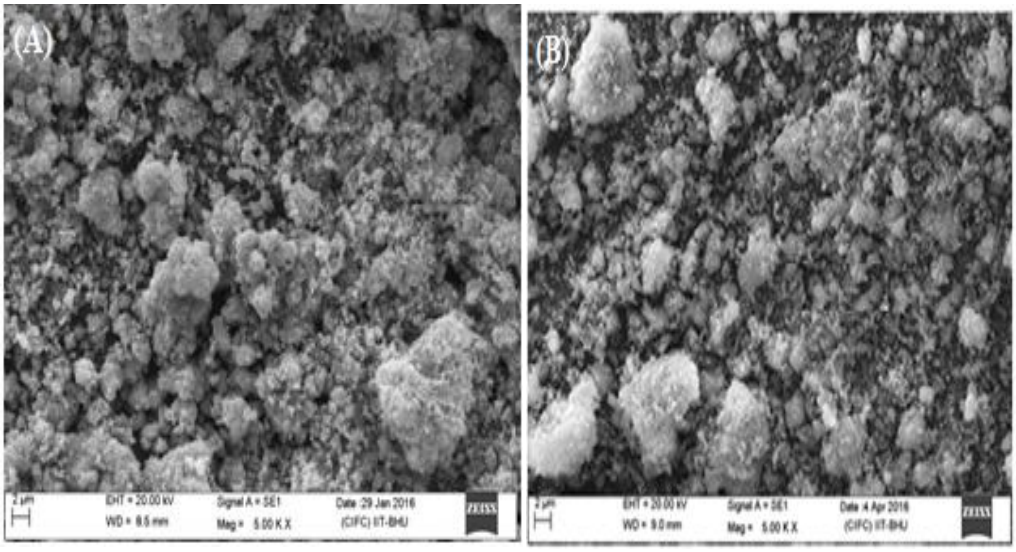

Figure 5.16 Scanning electron micrographs of LCos700 (A) and LMns700 (B)

5.3.1.2 Energy dispersive X-ray (EDX)

It was evident from the results of EDX analysis that all catalysts are pure due to the presence of only La, Co, Mn and O**.** There are no other elements present in the spectra as shown Figure 5.17 and Table 5.8 EDX results are also the good harmony with XRD results.

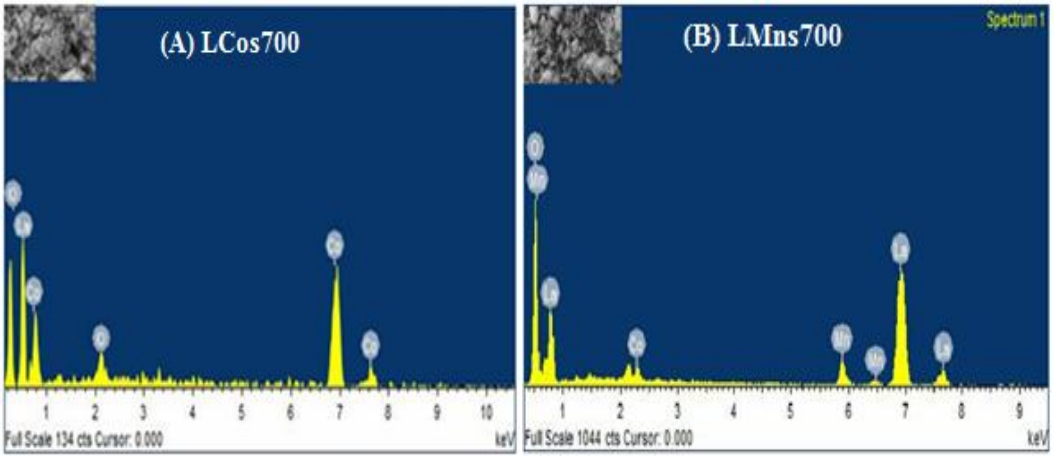

Figure 5.17 Energy dispersive X-ray spectra catalyst of (A) LCos700 and (B) LMns700

Table 5.8 Atomic % data of LCos700 and LMns700

LCos700				LMns700		
S.L.	Element	Weight%	Atomic%	Element	Weight%	Atomic%
1	O	12.68	54.24	O	22.98	65.66
2	Co	2.68	4.05	Mn	3.34	2.40
3	La	84.64	41.71	La	73.68	31.94
Total		100	100	Total	100	100

5.3.1.3 XRD analysis

X-ray diffraction (XRD) studies of the catalysts were carried out to identify the phase and structure of the catalysts. XRD patterns of different perovskite catalysts prepared by sol-gel method and calcinations with temperature 700°C. The detailed X-Ray diffraction patterns are shown in Figure 5.18. The 2-theta values for prepared perovskite show that these catalysts have rhombohedral perovskite phase (JCPDS 89-8775). The XRD location peak in XRD patterns of LCos700, and LMns700are almost same and LFes700 catalyst showing sharp peak comparing with these catalyst. Knowing the width of XRD peak and Scherrer equation, the calculated nano-crystalline is presented in Table 5.6.

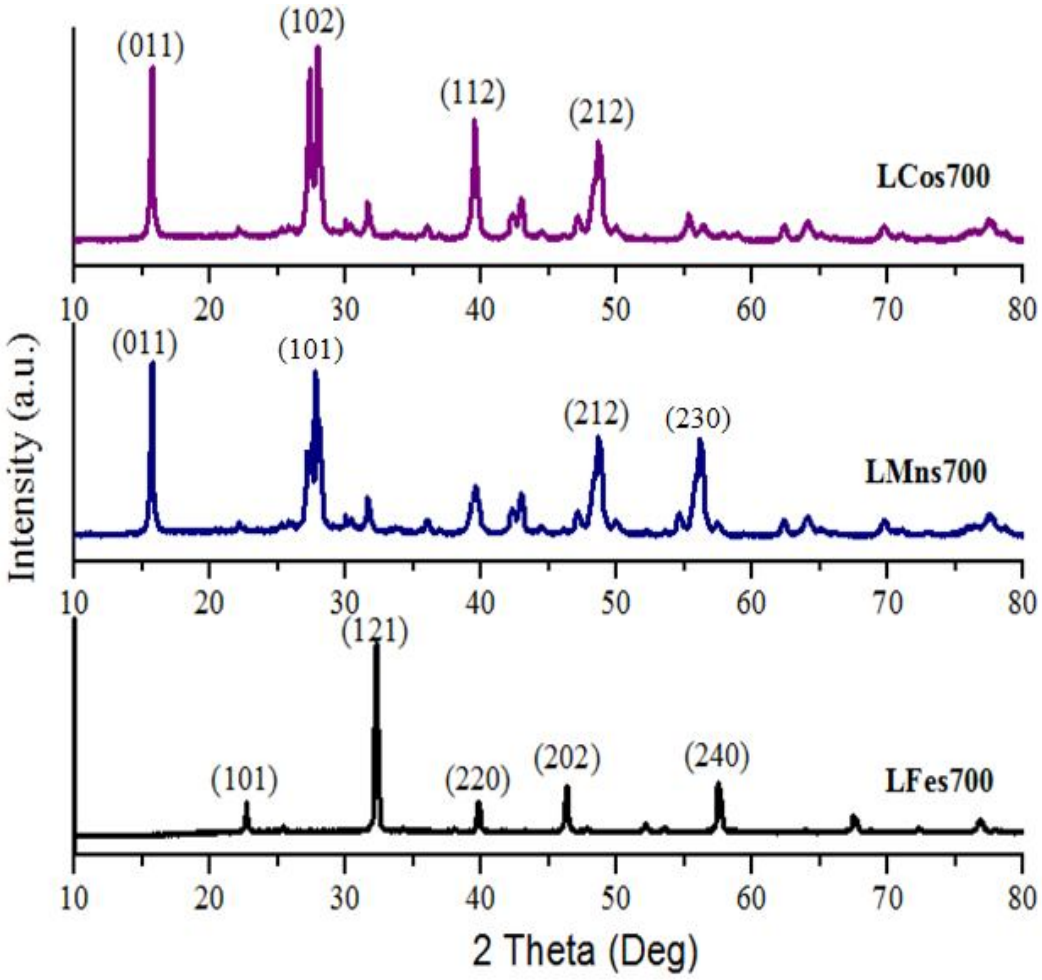

Figure 5.18 XRD of different perovskite catalysts

6.3.1.4 FTIR characterization

Figure 5.19 depicts the infrared absorption spectra of the $LaCoO_3$ catalyst prepared by sol-gel method and calcined at 700°C. The broad absorption bands around 3054 cm^{-1} and 2345 cm^{-1} appeared in the IR spectra of the as-prepared $LaCoO_3$ corresponded to OH stretching and OH bending of water. The absorption band at 1480 cm^{-1} corresponded to nitrate ion. In addition, the band at 1096 cm^{-1} was corresponded to Co-OH bending which is confirmed with the reported value that MOH bending mode appears below 1200 cm^{-1} [Nakamoto 1997]. The absorption band at 583 cm^{-1} in Figure 6.19 related to Co-O stretching vibration, which was confirmed with the reported value that cobalt-oxygen stretching appears at around 600 cm^{-1} [Khalil 2003].

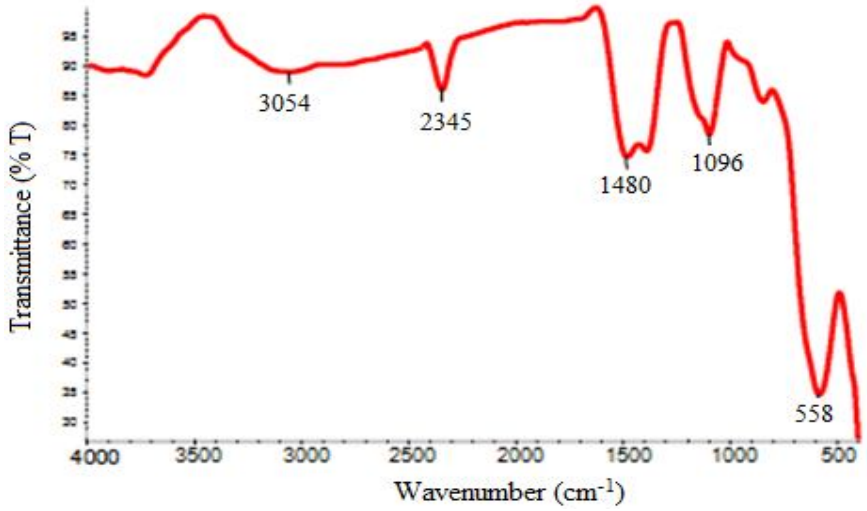

Figure 5.19 FTIR spectra of the $LaCoO_3$ catalyst

5.3.1.5 XPS analysis of the catalysts

The characteristic spectra collected for Co2p, and O1s in $LaCoO_3$ perovskite (LCos700) are displayed in Figure 5.20 (a), (b) respectively. On the basis of the binding energies of the Co2p main lines, as shown in Figure 5.21 (b), it is difficult to determine the oxidation states of cobalt cations because similar values can be obtained for most of the cobalt oxides and hydroxides (e.g. CoO, Co_2O_3, Co_3O_4, and CoOOH). It is reported that the ΔE value of spin-orbit splitting for CoO is 16.0 eV, and that of Co_2O_3 is 15.0 eV [Cesar 2000]. For Co_3O_4 with the mixed valence of Co ions, a spin-orbit splitting value of 15.2eV has been reported [Ichimura *et al.,* 1980]. It collects all the binding energy and spin-orbit splitting values of Co for the $LaCoO_3$ perovskite catalyst. The Co 2p XPS spectra of the catalyst consist of two main lines with the spin-orbit splitting (ΔE) falling in the range of Co_3O_4, implying that the cobalt ions exist in the mixed valence states of +2 and +3. As a result of high-valent Co ion, oxygen vacancies are created which accumulates a large number of adsorption oxygen on the surface.

The O1s energy spectrum, Figure 5.20(b) consists of two peaks, which correspond to two forms of oxygen, i.e. lattice oxygen O_{lat} and adsorption oxygen O_{ads}

on the sample surface. The peak at the binding energy of 527.5-530 eV corresponds to the lattice oxygen species (O^{2-}, O^{-}), which reflect the redox behavior of the metal, and the peak at 530-531.5 eV corresponds to the adsorption oxygen species (O_2^{-}, O_2^{2-}), that is the active centre for the oxidation.

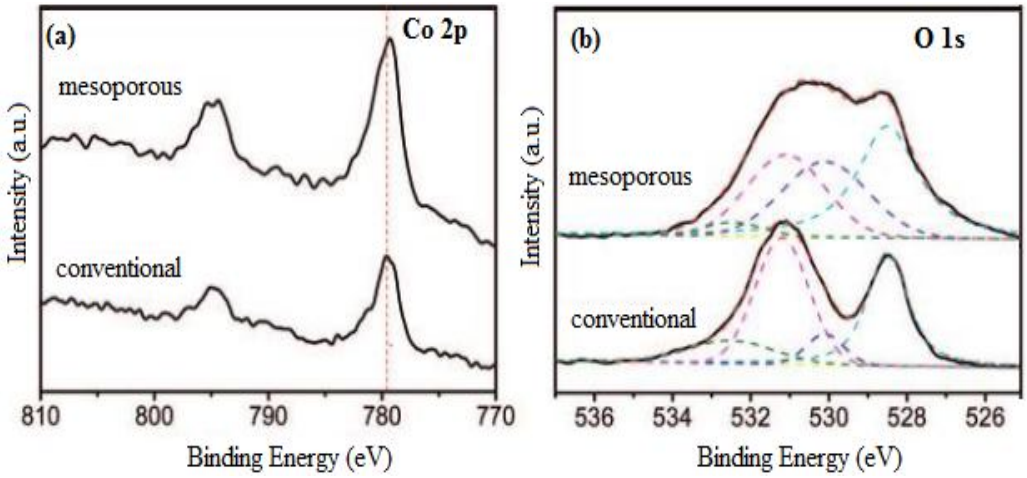

Figure 5.20 XPS spectra of the Co2p (a) and (b) O1s levels of LCos700

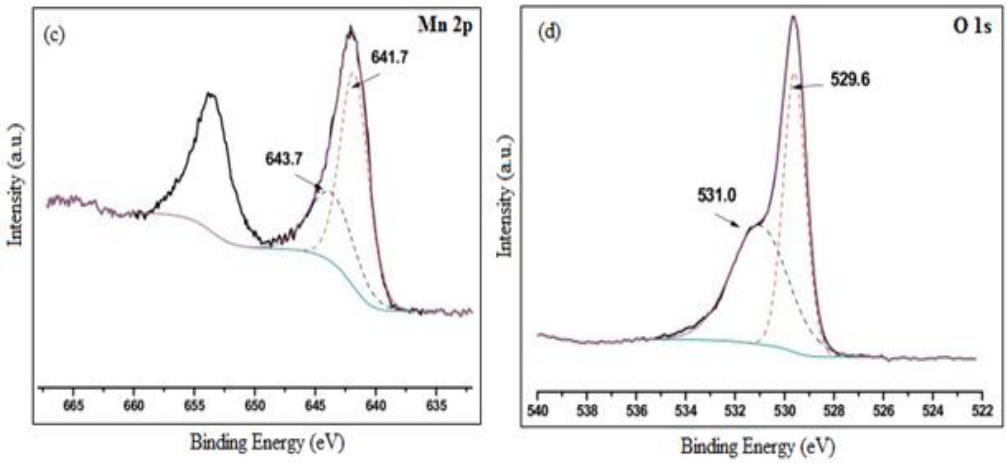

Figure 5.21 XPS spectra of fresh LMns700 (c) Mn 2 p and (d) O 1s

The valance states of the elements were characterized by XPS. The results are reported in Figure 5.21 (c) and (d). For the Mn 2 p spectrum of $LaMnO_3$ (LMns700), the peaks at 643.7 and 641.7 eV were corresponded to Mn^{4+} and Mn^{3+}, respectively [Yan *et al.*, 2009]. The ratio of Mn^{4+}/Mn^{3+} was determined to be 33.93/66.07. A higher valence state of Mn may result in a higher catalytic oxidation

activity [He *et al.*, 2014]. The state of O was also evaluated by XPS analysis, as shown in Figure 5.21 (d), in the O 1s spectrum of $LaMnO_3$, the peaks located at 531.0 and 529.6 eV were ascribed to the lattice oxygen (O_{latt}) and adsorbed oxygen (O_{ads}), respectively.

5.3.2 Catalysts activity tests for simultaneous combustion of soot and reduction NO

5.3.2.1 Soot combustion

The prepared LCos700, LMns700 catalysts were examined to check the better activity for simultaneous reduction of soot and NO. The activity for soot combustion is shown in Figure 5.22 and Table 5.9, which indicates that LFes700 catalyst is showing better activity as compared with the LCos700, LMns700 catalysts.

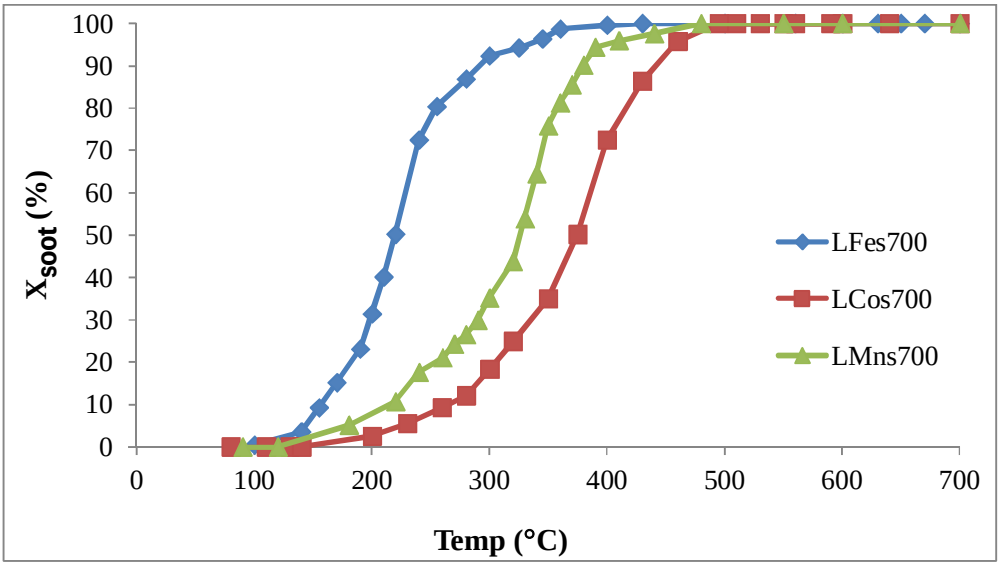

Figure 5.22 Soot conversion activity of different perovskite catalyst

Table 5.9 Comparison of activity soot and NO conversion of different pure catalysts

S. N.	Catalyst	Soot oxidation				NO reduction	
		T_{10} (°C)	T_{50} (°C)	T_{100} (°C)	T_p (°C)	T_{max} (°C)	X_{NO} (%)
1.	**LFes700**	**168**	**218**	**429**	**323**	**325**	**54**
2.	LCos700	273	372	489	428	374	51
3.	LMns700	215	324	482	369	349	48.61

5.3.2.2 NO reduction

The prepared LCos700, LMns700 catalysts were examined to check the better activity for simultaneous reduction of soot and NO. The activity NO conversion is shown in Figure 5.23, which indicates that LFes700 catalyst is showing better activity as compared with the LCos700, LMns700 catalysts.

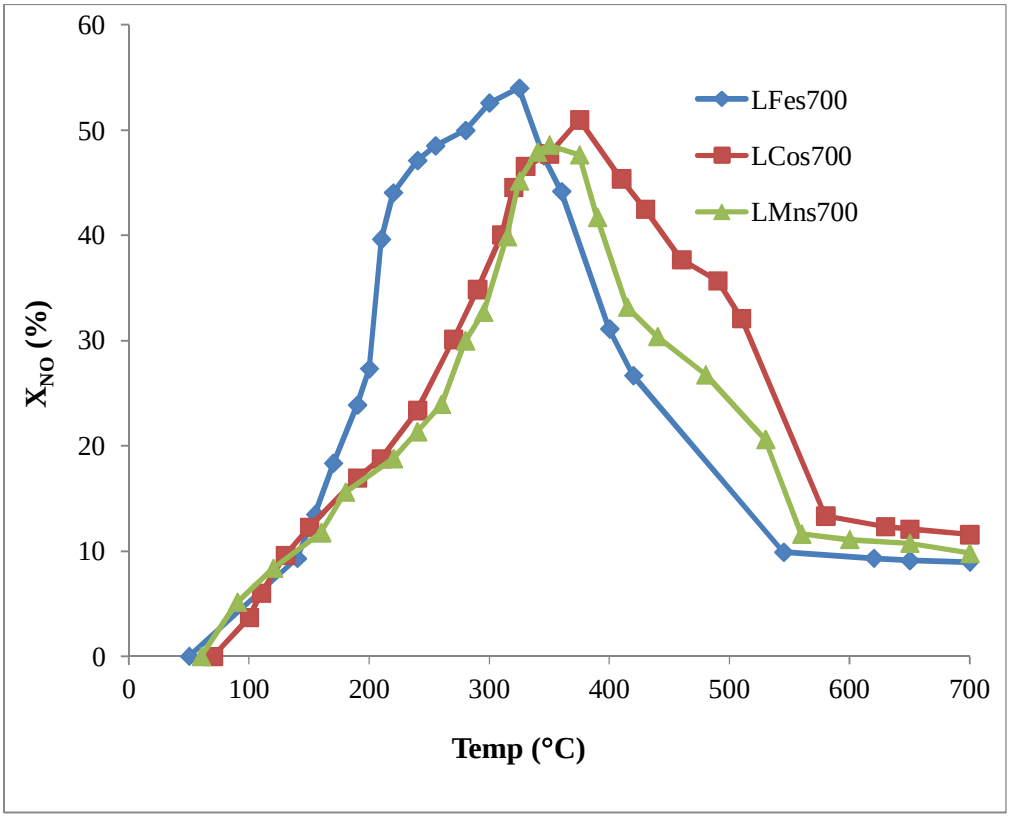

Figure 5.23 NO conversion activity of different perovskite catalyst

5.4 Comparison between $LaFeO_3$ with A-site substitution of K

To further enhance the activity of $LaFeO_3$ catalyst, A-site was substituted with K, because K gives excellent activity which was confirmed in literature by Mescia *et al.*, 2008, Liu *et al.*, 2012 and Zhen *et al.*, 2015.

5.4.1 Structural and morphological characterization of catalysts

5.4.1.1 Scanning electron microscope (SEM) characterization results

The SEM image of LKFes700 (A-site substitution of K) catalyst is prepared by sol-gel methods and compared with the LFes700 at calcination temperature 700°C. The SEM micrographs at 10 KX magnifications shown in Figure 5.24 revealed that the prepared catalyst sample was highly porous and aggregated than the LFes700. The morphologies of particles are irregular shape; granular particles were also between 40 and 100 nm calculated by "Image J software" with varying degree of agglomeration.

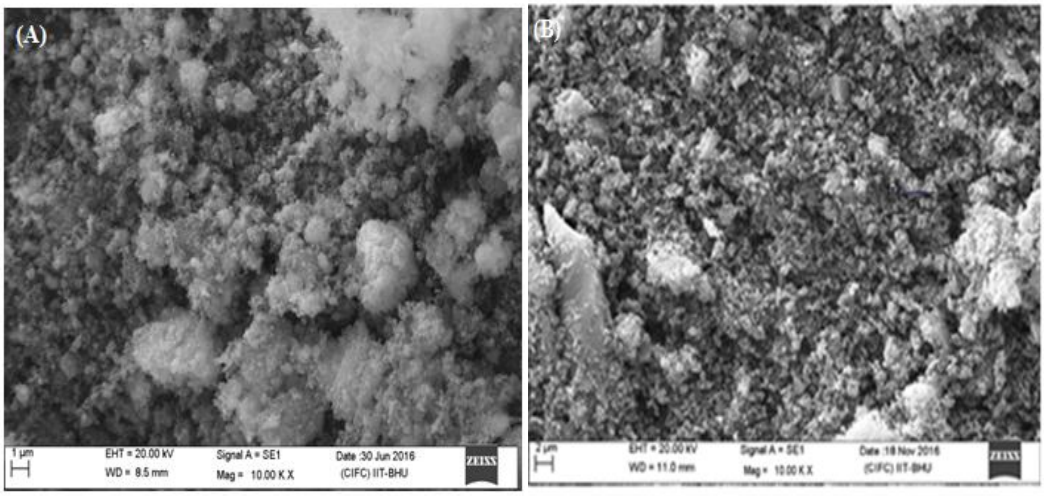

Figure 5.24 Scanning electron micrographs of (A) LFes700 and (B) LKFes700

6.4.1.2 Energy dispersive X-ray (EDX)

It was evident from the results of EDX analysis that all catalysts are pure due to the presence of only La, K, Fe, and O**.** There are no other elements present in the spectra as shown Figure 5.25 EDX results are also the good harmony of XRD results.

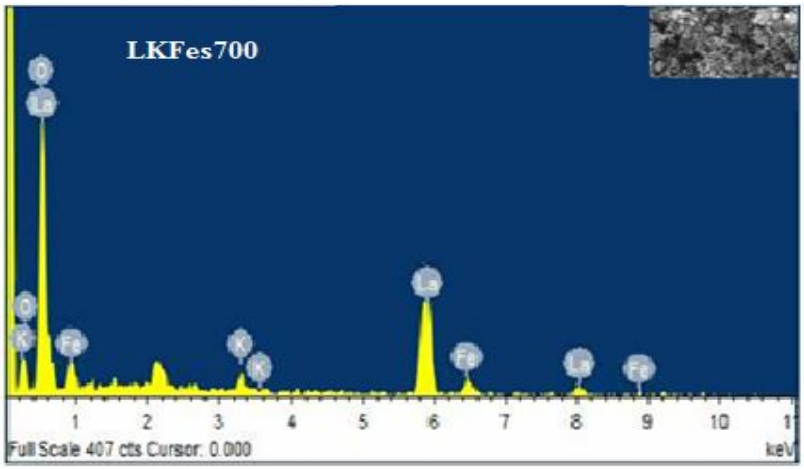

Figure 5.25 Energy dispersive X-ray spectra catalyst of LKFes700

Table 5.10 Atomic % data of LKFes700

S.L.	Element	Weight%	Atomic%
1	O K	53.46	60.89
2	K K	10.33	9.79
3	Fe K	8.76	11.34
4	La K	28.45	17.98
Totals		100.00	100

5.4.1.3 XRD analysis

X-ray diffraction (XRD) studies of the catalysts were carried out to identify the phase and structure of the catalysts. XRD patterns of K-substitution of pure $LaFeO_3$ catalysts prepared by sol-gel method and calcinations with temperature 700°C. The detailed X-Ray diffraction patterns are shown in Figure 5.26. The 2-theta values for prepared perovskite show that these catalysts have rhombohedral perovskite phase (JCPDS 89-8775). The XRD location peak in XRD patterns of LKFes700 catalyst showing sharper peak than LFes700 catalyst. Knowing the width of XRD peak and Scherrer equation, the calculated nano-crystalline is presented in Table 5.6. K substitution is confirmed with an addition peak at 25.06°.

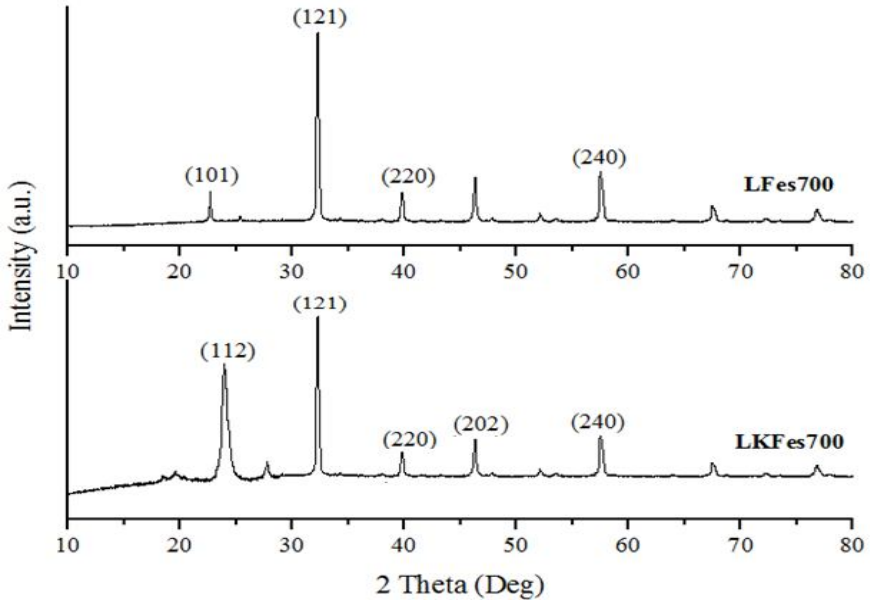

Figure 5.26 XRD comparison between pure perovskite and A-site K substituted catalysts

5.4.1.4 FTIR characterization

Figure 5.27 depicts the infrared absorption spectra of the LKFes700 catalyst prepared by sol-gel method and calcined at 700°C. The broad absorption bands around 3140 cm^{-1} and 567 cm^{-1} appeared in the IR spectra. The absorption band at 1470 cm^{-1} corresponded to nitrate ion. In addition, the band at 1120 cm^{-1} was corresponded to Fe-OH bending which is confirmed with the reported value that MOH bending mode appears below 1200 cm^{-1} [Nakamoto 1997].

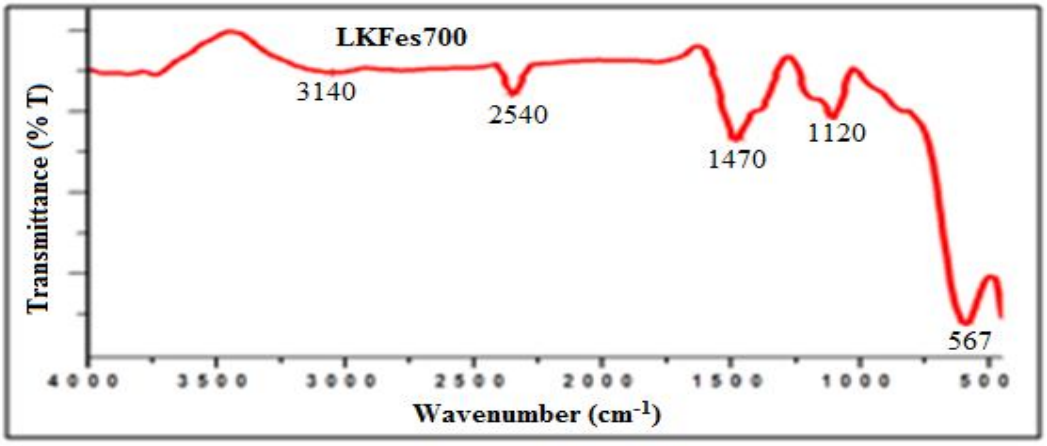

Figure 5.27 FTIR of LKFes700 catalyst

5.4.1.5 XPS analysis of the catalysts

The characteristic spectra collected for La3d, K2p, Fe 2p and O1s in LKFes700 perovskite are displayed in Figure 5.28 (a), (b) (c), and (d) respectively. On the basis of the binding energies of the K 2p main lines, as shown in Figure 5.28 (b), it is difficult to determine the oxidation states of potassium cations because similar values can be obtained for most of the potassium oxides and hydroxides. The Fe 2p XPS spectra of the catalyst consist of two main lines with the spin-orbit splitting (ΔE), implying that the cobalt ions exist in the mixed valence states of +2 and +3. As a result of high-valent Fe ion, oxygen vacancies are created which accumulates a large number of adsorption oxygen on the surface.

The O1s energy spectrum, Figure 5.28 (d) consists of two peaks, which correspond to two forms of oxygen, i.e. lattice oxygen O_{lat} and adsorption oxygen O_{ads} on the sample surface. The peak at the binding energy of 733.67-715.94 eV corresponds to the lattice oxygen species (O^{2-}, O^{-}).

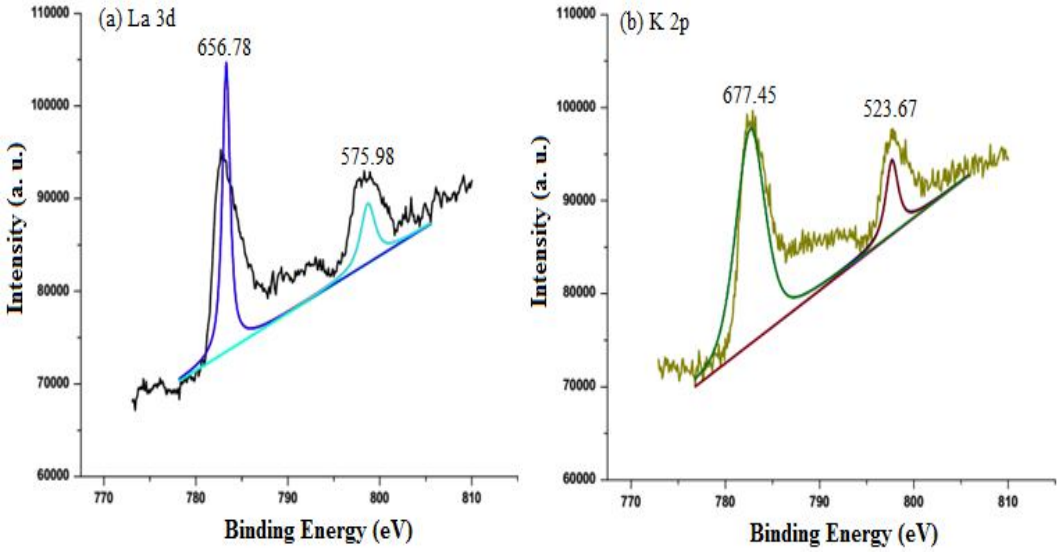

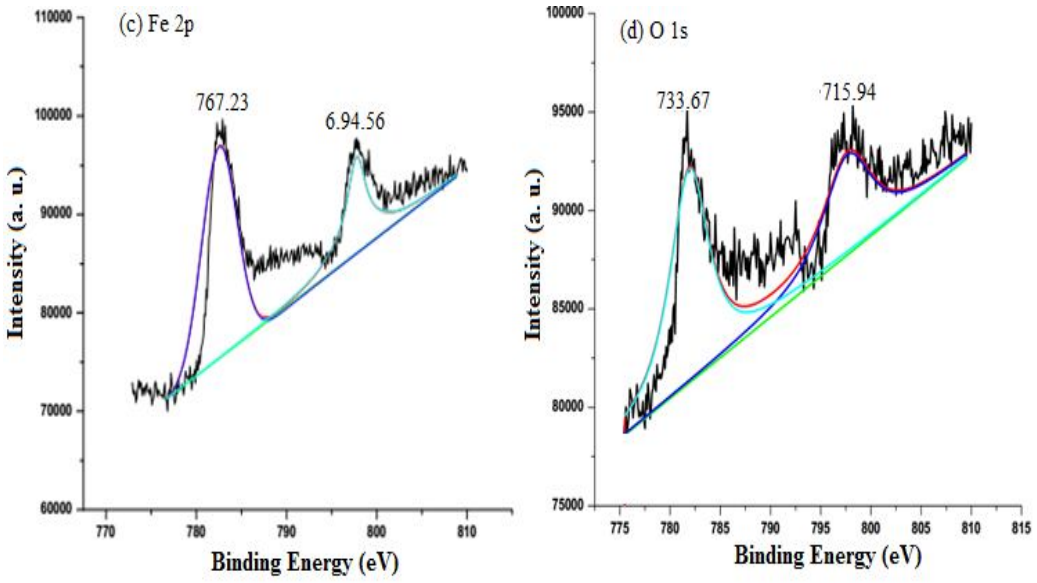

Figure 5.28 XPS spectra of fresh LKFes700 catalyst,(a) La 3d, (b) K 2p, (c) Fe 2p, (d) O 1s

5.4.2 Catalysts activity tests for simultaneous combustion of soot and NO reduction

5.4.2.1 Soot combustion

The experiment was conducted to check the effect with A-site K substitution catalyst effect on $LaFeO_3$ perovskite (LKFes700) for simultaneous reduction of soot and NO. It can be seen from the Figure 5.29 and Table 5.11 that the 10%, 50%, 100% oxidation of diesel soot over different catalyst LKFes700 initiated at different temperatures of 124, 213, and 407°C respectively which is within the temperature window of diesel exhaust. The A-site substitution of K has enhanced the oxidation activity of soot with total conversion at 407°C.

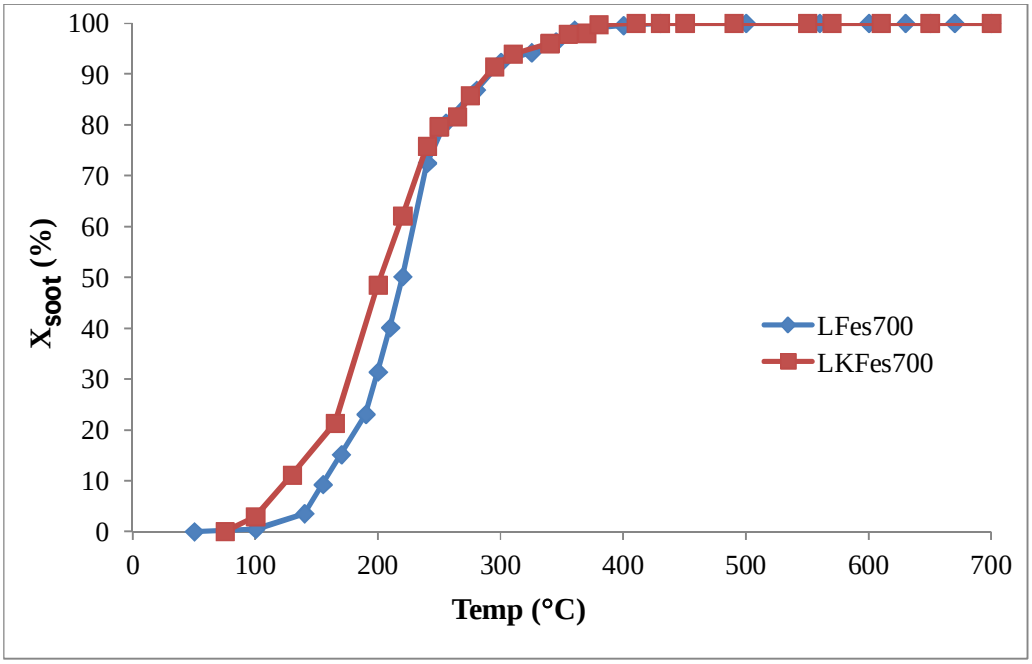

Figure 5.29 Soot conversion activity, comparison between pure perovskite and A-site K substituted catalysts

Table 5.11 Comparison with pure $LaFeO_3$ with A-site K substitution catalyst

S. N.	Catalyst	Soot oxidation				NO reduction	
		T_{10} (°C)	T_{50} (°C)	T_{100} (°C)	T_p (°C)	T_{max} (°C)	X_{NO} (%)
1.	LFes700	168	218	429	323	325	54
2.	**LKFes700**	**124**	**213**	**407**	**339**	**340**	**59.29**

5.4.2.2 NO reduction

The experiment was conducted to check the effect with A-site K substitution catalyst effect on $LaFeO_3$ perovskite (LKFes700) for simultaneous reduction of soot and NO. It can be seen from the Figure 5.30 that the maximum reduction NO over different catalyst LKFes700 is 59.29% at 340°C which is within the temperature window of diesel exhaust. The A-site substitution of K is enhanced the reduction activity NO with 59.29% but at higher temperate of 340°C.

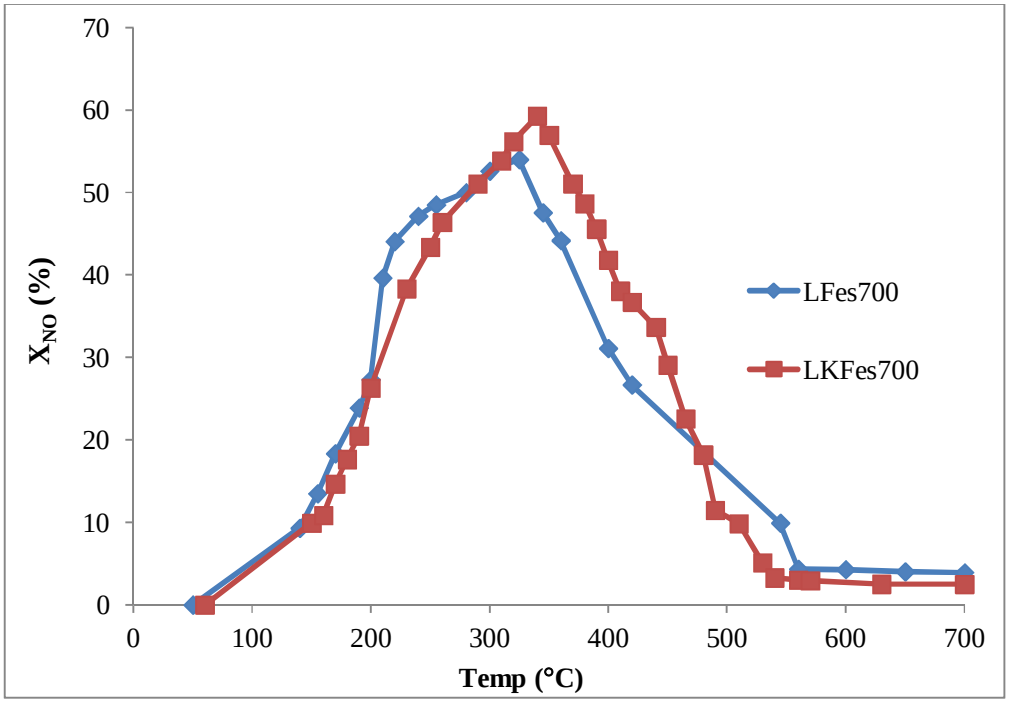

Figure 5.30 NO conversion activity, comparison between pure perovskite and A-site K substituted catalysts

5.5 Double substitution of $LaFeO_3$ with A-site K and B-site Cu

For higher NO reduction activity at lower temperature $LaFeO_3$ was double substituted with K and Cu at A and B-sites respectively.

5.5.1 Structural and morphological characterization of catalysts

5.5.1.1 Scanning electron microscope (SEM) characterization results

The SEM images of LKFeCus700-A, LKFeCus-B and LKFeCus-C prepared by the sol-gel method following the calcination at 700°C. The SEM micrographs at 5 KX magnifications shown in Figure 5.31 revealed that the prepared catalyst samples were highly porous and aggregated. The morphologies of particles are irregular shape; granular particles were also between 40 and 100 nm calculated by "Image J software" with varying degree of agglomeration. In comparison to all the prepared catalysts, LFeCus700-B was more aggregated and porous surface as shown in Figure 5.31 (A, B, and C).

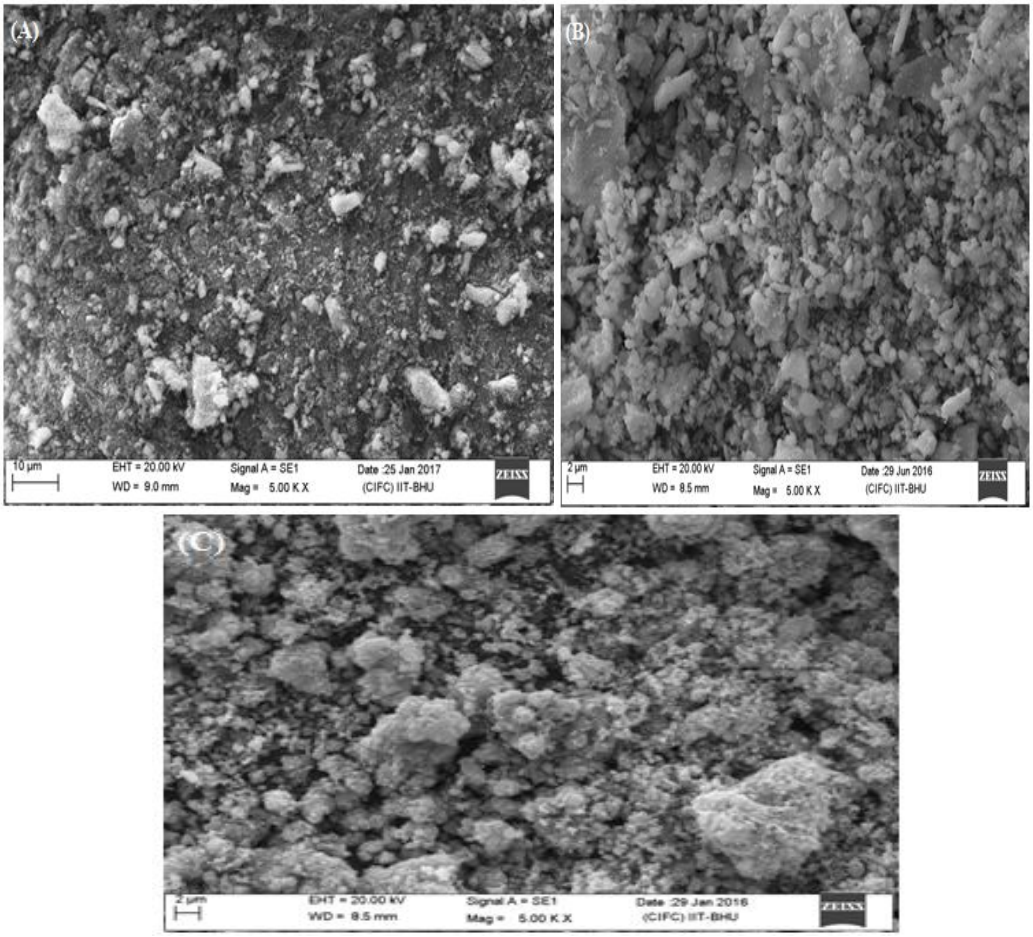

Figure 5.31 Scanning electron micrographs of (A) LKFeCus700-A, (B) LKFeCus700-B, (C) LKFeCus700-C

5.5.1.2 Energy dispersive X-ray (EDX)

It was evident from the results of EDX analysis that all catalysts are pure due to the presence of only La, K, Fe, Cu and O**.** There are no other elements present in the spectra as shown in Figure 5.32 and Table 5.12 EDX results are also the good harmony with XRD results.

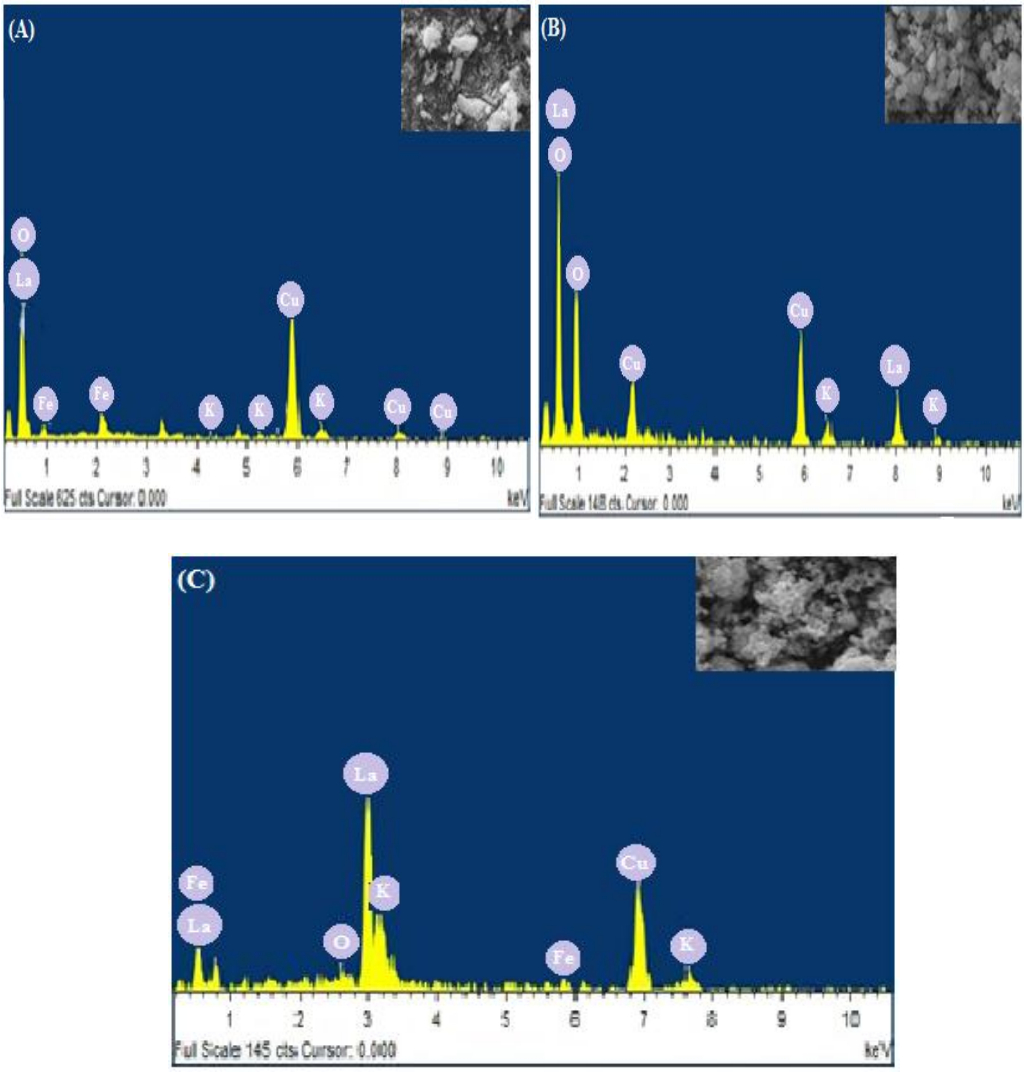

Figure 5.32 Energy dispersive X-ray spectra catalyst of (A) LKFeCus700-A, (B) LKFeCus700-B, (C) LKFeCus700-C

Table 5.12 Atomic % data of LKFeCus700-A, LKFeCus700-B, LKFeCus700-C

LKFeCus700-A				**LKFeCus700-B**		**LKFeCus700-C**	
S.L.	Element	Weight%	Atomic%	Weight%	Atomic%	Weight%	Atomic%
1	O	27.29	62.60	22.51	57.08	25.98	65.66
2	Cu	2.79	1.84	3.30	2.40	3.95	3.45
3	Fe	4.80	2.99	4.86	3.34	5.65	3.16
4	K	31.28	18.91	31.55	21.99	29.91	19.57
5	La	33.84	13.66	37.79	6.20	34.51	8.16
Total		100	100	100	100	100	100

5.5.1.3 XRD analysis

X-ray diffraction (XRD) studies of the catalysts were carried out to identify the phase and structure of the catalysts. XRD patterns of A-site substitution of K and B-site substation Cu of $LaFeO_3$ catalysts prepared by sol-gel method and calcinations at temperature 700°C. The detailed X-Ray diffraction patterns are shown in Figure 5.33. The 2-theta values for prepared perovskite show that these catalysts have rhombohedral perovskite phase (JCPDS 89-8775). The XRD location peak in XRD patterns of LKFeCus700-A, LKFeCus700-B, LKFeCus700-C catalysts showing almost same peaks. Knowing the width of XRD peak and Scherrer equation, the calculated nano-crystaline is presented in Table 5.13.

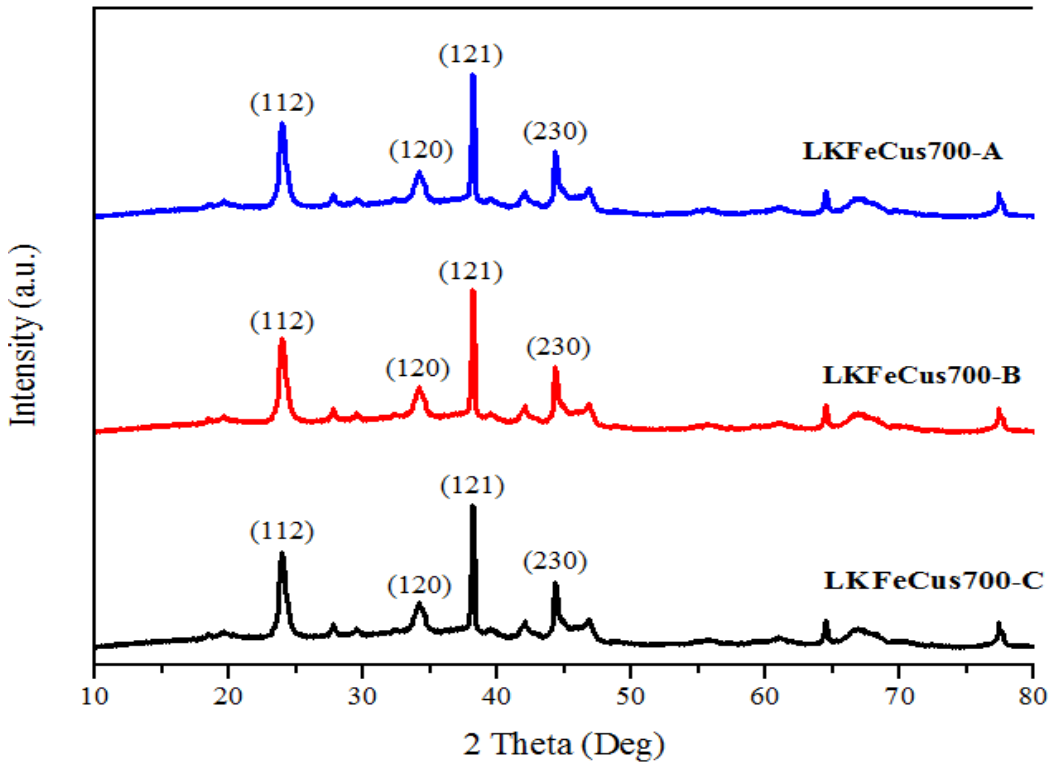

Figure 5.33 XRD of LKFeCus700-A, LKFeCus700-B, LKFeCus700-C

Table 5.13 Textural characterization of substituted perovskite catalyst samples

Catalyst sample	Surface area (m^2/g)	Pore volume (cm^3/g)	Average pore dia. (nm)	Crystallite size (nm)
LKFes700	16.23	0.0058	31.66	59.66
LKFeCus700-A	19.79	0.0056	30.13	54.34
LKFeCus700-B	**23.81**	**0.0062**	**27.52**	**42.57**
LKFeCus700-C	20.04	0.0053	29.01	45.23
LKFeCos700	17.62	0.0046	30.86	51.22
LKFeCus700-D	22.76	0.0048	28.24	46.34
LKFeCus700-E	**25.11**	**0.0067**	**23.58**	**38.21**

5.5.1.4 FTIR characterization

Figure 5.34 (a), (b), and (c) depicts the infrared absorption spectra of the LKFeCus700-A, LKFeCus700-B, and LKFeCus700-C catalysts prepared by sol-gel method and calcined at 700°C. The broad absorption bands around 3600 cm^{-1} and 503 cm^{-1} appeared in the IR spectra. The absorption bands at 2156 cm^{-1} (Figure 5.34 a), 2254 cm^{-1} (Figure 5.34 b), and 2360 cm^{-1} (Figure 5.34 c) corresponded to nitrate ion. In addition, the bands at 1178 cm^{-1} (Figure 5.34 a), 1231 cm^{-1} (Figure 5.34 b), and 1250 cm^{-1} (Figure 5.34 c) were corresponded to Fe-OH bending which is confirmed with the reported value that MOH bending mode appears below 1200 cm^{-1} [Nakamoto 1997].

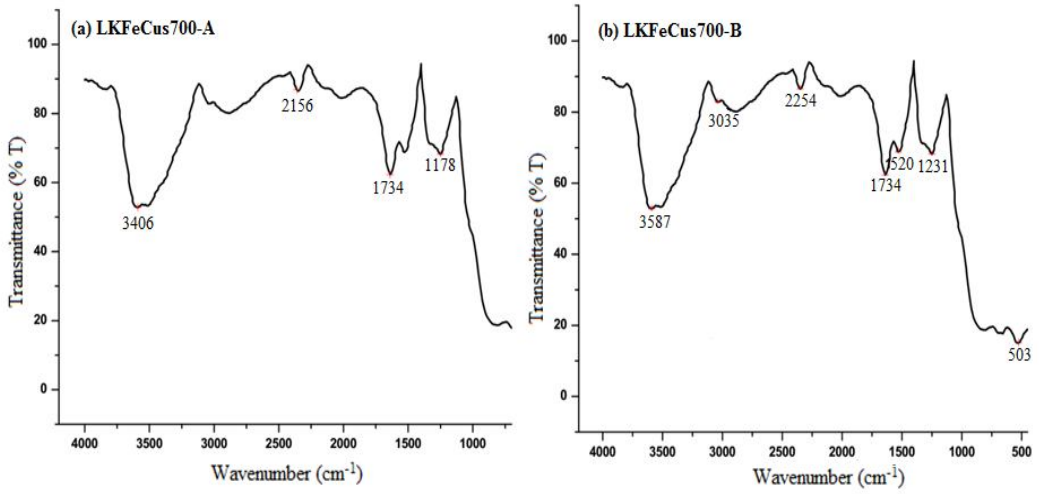

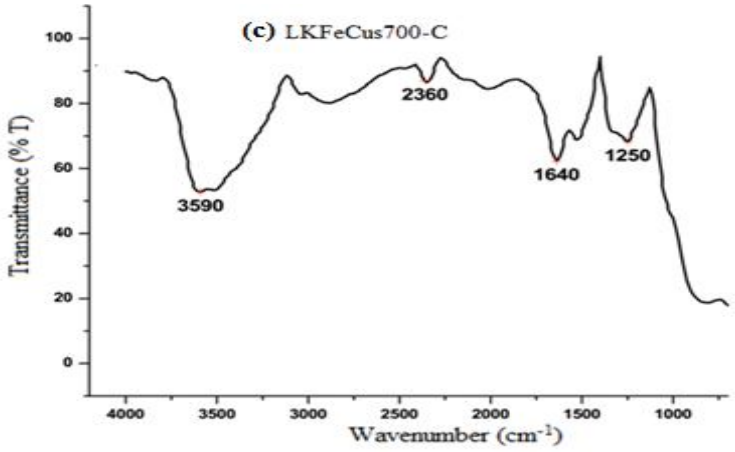

Figure 5.34 FTIR of catalyst (a) LKFeCus700-A, (b) LKFeCus700-B, (c) LKFeCus700-C

5.5.1.5 XPS analysis of the catalysts

The characteristic spectra collected for La3d, K2p, Fe2p, Cu2p and O1s in LKFeCus700-B perovskite catalyst is displayed in Figure 5.35 (a), (b) (c), (d), and (e) respectively. The high-resolution spectrum of La 3d (Figure 5.35 a) is showed two strong La peaks at 658.43 and 566.27 eV corresponding to spin-orbit splitting of $3d_{5/2}$ and $3d_{3/2}$ of La^{3+} ions in oxide form. On the basis of the binding energies of the K 2p main lines, as shown in Figure 5.35 (b), it is difficult to determine the oxidation states of cobalt cations because similar values can be obtained for most of the cobalt oxides and hydroxides. The Fe 2p XPS (Figure 5.35 c) spectra of the catalyst consists of two main lines with the spin-orbit splitting (ΔE), implying that the cobalt ions exist in the mixed valence states of +2 and +3. As a result of high-valent Fe ion, oxygen vacancies are created which accumulates a large number of adsorption oxygen on the surface. The Cu 2p XPS (Figure 5.35 d) spectra of the catalyst consist of two main lines with the spin-orbit splitting (ΔE), implying that the cobalt ions exist in the mixed valence states of +2 and +3 and the peaks lie in between 950.51-931.72 eV.

The O1s energy spectrum, Figure 5.35 (e) consists of two peaks, which correspond to two forms of oxygen, i.e. lattice oxygen O_{lat} and adsorption oxygen O_{ads}

on the sample surface. The peak at the binding energy of 735.31-703.86 eV corresponds to the lattice oxygen species (O^{2-}, O^{-}).

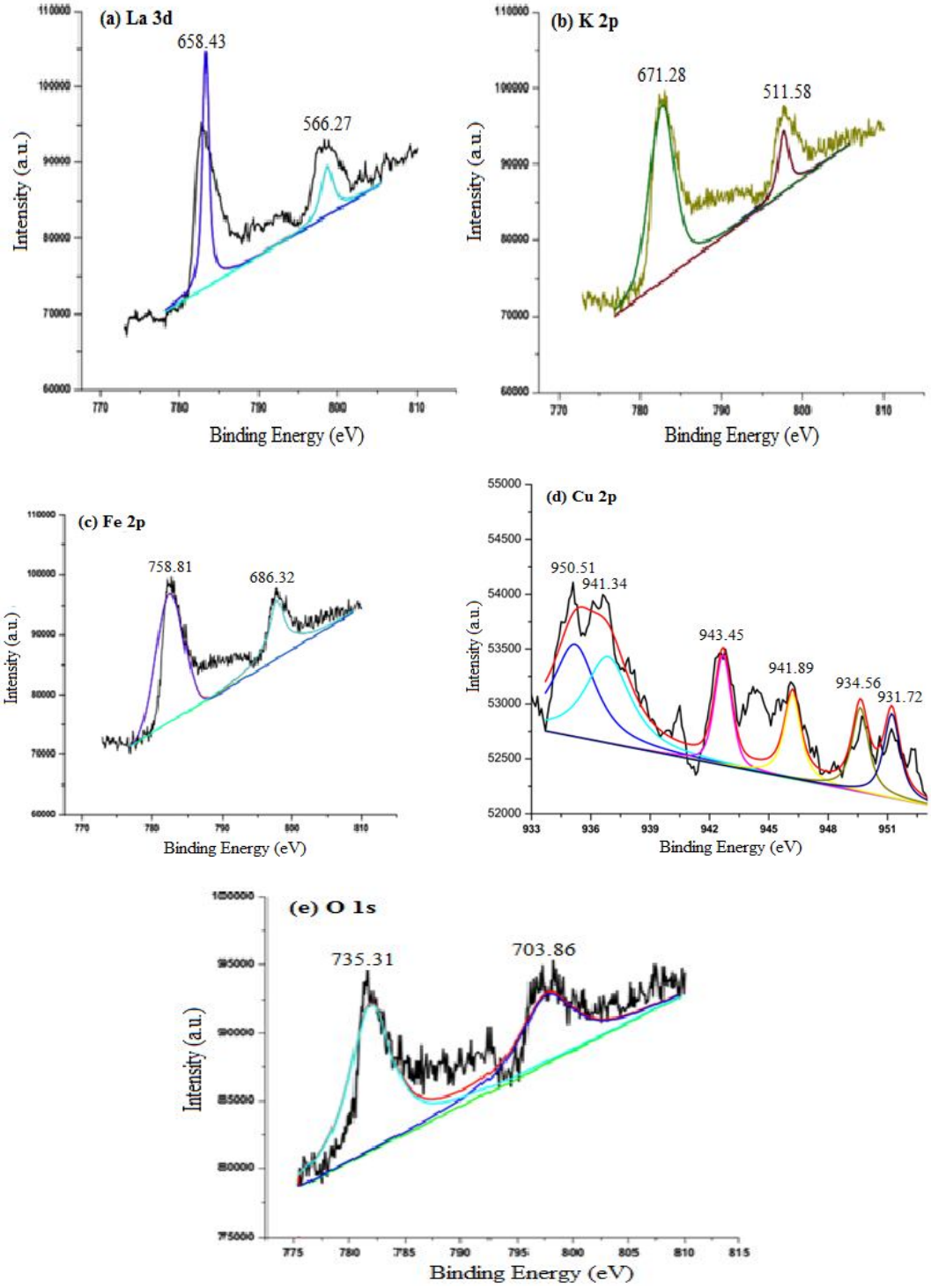

Figure 5.35 XPS study of LKFeCus700-B; (a) La 3d, (b) K 2p, (c) Fe 2p, (d) Cu 2p, (e) O 1s

5.5.1.6 Surface area and textural properties of LKFeCus700-B

Low temperature (-196°C) nitrogen adsorption isotherms were used for the determination of the textural properties of the catalysts synthesized. The textural parameters including BET surface area, total pore volume and pore diameter of the catalysts are summarized in Table 5.12. The typical isotherm of LKFeCus700-B is shown in Figure 5.36 which is of type IV of IUPAC classification 1984. This type of isotherm occurs on porous adsorbent with pores in the range of 1.5-100 nm. The average pore diameter obtained by BET analysis suggests that catalyst was mesoporous. The initial part of the isotherm is attributed to monolayer adsorption. At higher pressures the slope shows increased uptake of adsorbate as the pores become filled, inflection point typically occurs near the completion of the first monolayer. In the mesoporous materials, due to larger pores, the greater number of molecules interacts with each other and displays better catalytic activity. Hysteresis loops occur at low relative pressures (around 0.4) and an area within the loop is very small suggesting open cylindrical pores of the catalyst. The catalyst with copper substitution 0.15% has the highest surface area.

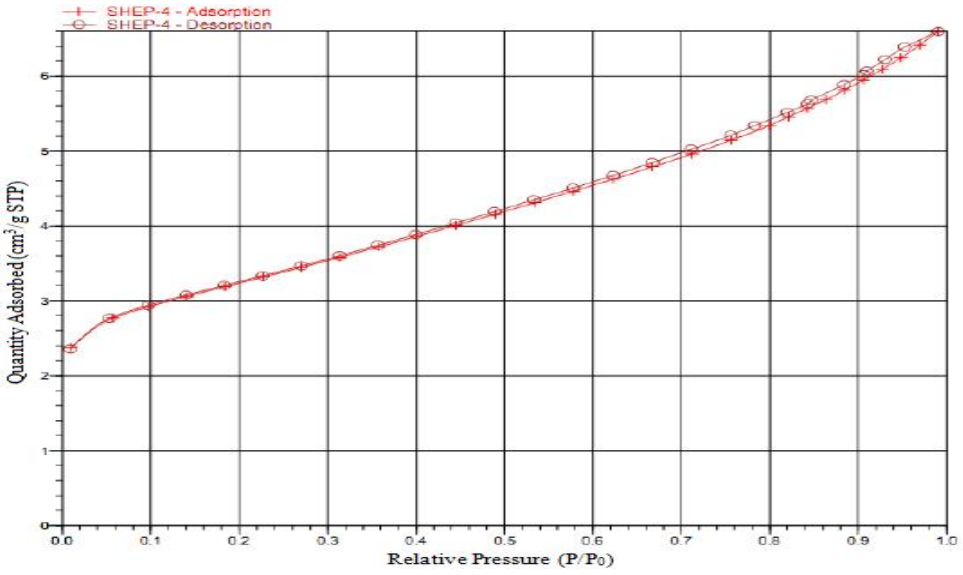

Figure 5.36 Nitrogen adsorption-desorption isotherm for LKFeCus700-B catalyst

5.5.2 Catalysts activity tests for simultaneous combustion of soot and reduction NO

5.5.2.1 Soot combustion

The series of experiments A-site potassium (K) and B-site copper (Cu) substitution of $LaFeO_3$ perovskite catalyst was conducted for simultaneous reduction of soot and NO. The three catalysts LKFeCus700-A, LKFeCus700-B, and LKFeCus700-C have been different copper concentration of 10, 15, and 20% were showing excellent results soot oxidation activity. The catalyst having copper concentration of 15% is showing best activity at lower temperature of 363°C. All catalysts are showing total combustion of the soot < 500°C, i.e. within the temperature window of diesel exhaust. It can be seen from the Figure 6.37 that the T_{10}, T_{50}, $T_{100,}$ and Tp oxidation of diesel soot over the LKFeCus700-B catalyst was 133, 207, 363, and 326°C respectively. The catalytic activity of the catalyst samples chiefly depends on three factors: chemical composition, the degree of crystallinity, and the crystals morphology (including particle sizes, pore size distribution, and specific surface area of the perovskite catalyst).

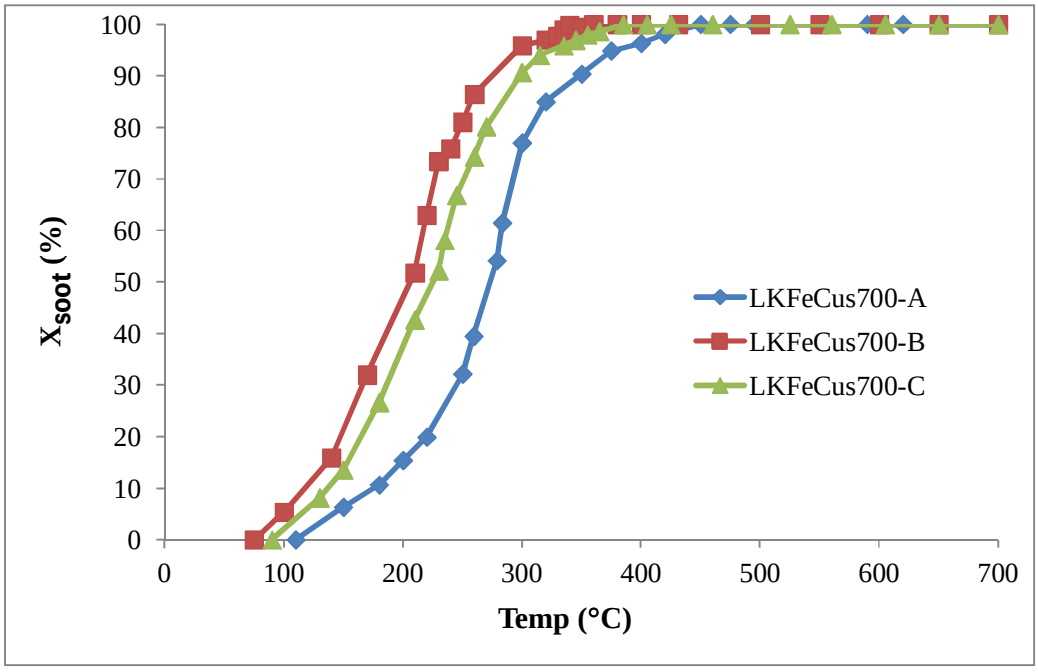

Figure 5.37 Soot conversion activity of LKFeCus700-A, LKFeCus700-B, LKFeCus700-C

5.5.2.2 NO reduction

The series of experiments A-site potassium (K) and B-site copper (Cu) substitution of $LaFeO_3$ perovskite catalyst was conducted for simultaneous reduction of soot and NO. The three catalysts LKFeCus700-A, LKFeCus700-B, and LKFeCus700-C were showing an excellent result for NO reduction activity but LKFeCus700-B was the best among all. All the catalysts showed total reduction of NO < 500°C, i.e. within the temperature window of diesel exhaust. It can be seen from the Figure 5.38 that the $T_{max\text{-}NO}$ for NO reduction over the LKFeCus700-B catalyst at 369°C was 71.41%.

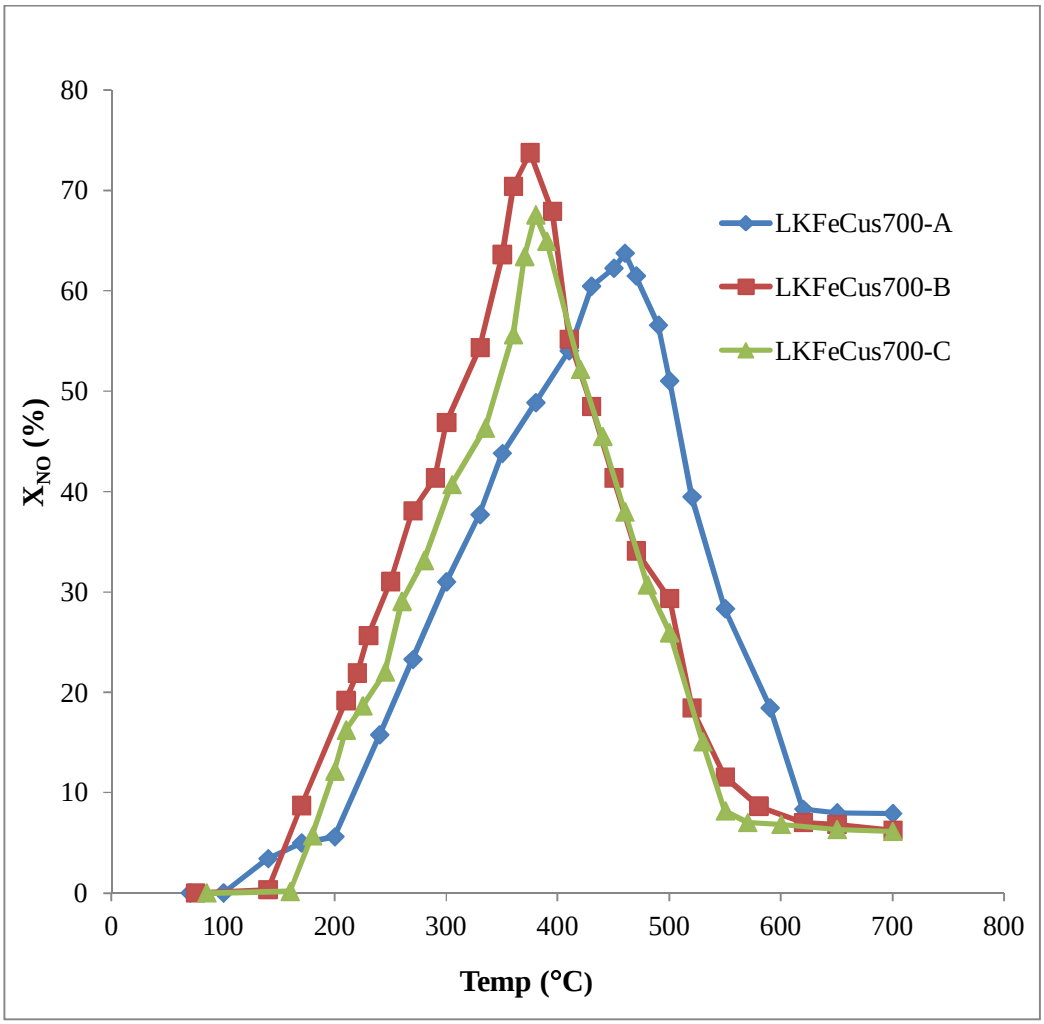

Figure 5.38 NO conversion activity of LKFeCus700-A, LKFeCus700-B, LKFeCus700-C

5.6 Comparison of B-site substitutions of Co

LCos700 catalyst was giving comparable activity LFes700 for simultaneous soot NO removal. This shows that cobalt can be considered for the control of soot-NO emissions. Therefore B-site of the catalyst was substituted with cobalt.

5.6.1 Structural and morphological characterization of catalysts

5.6.1.1 Scanning electron microscope (SEM) characterization results

The SEM image of LKFeCos700 catalyst was prepared by the sol-gel method by keeping same calculation temperature with LKFeCus700-B. The SEM micrographs at 5KX magnifications shown in Figure 5.39 revealed that the prepared catalyst samples were highly porous and aggregated. The morphologies of particles are irregular shape; granular particles were also between 40 and 100 nm calculated by "Image J software" with varying degree of agglomeration. In comparison with LKFeCus700-B catalyst, it has uniform and porous surface.

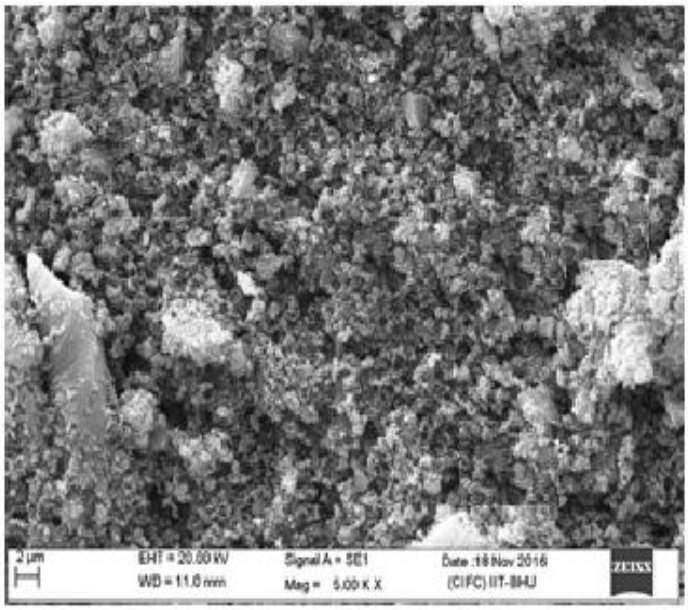

Figure 5.39 Scanning electron micrographs of LKFeCos700

5.6.1.2 Energy dispersive X-ray (EDX)

It was evident from the results of EDX analysis that all catalysts are pure due to the presence of only La, K, Fe, Co and O**.** There are no other elements present in the spectra as shown Figure 5.40 EDX results are also the good harmony with XRD results.

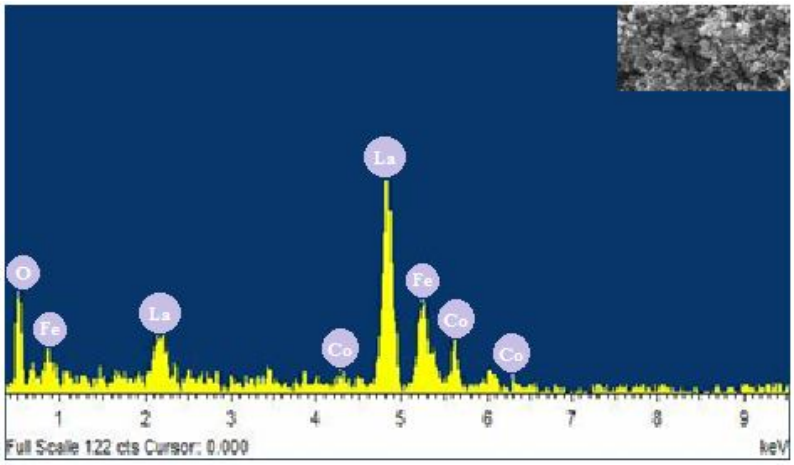

Figure 5.40 Energy dispersive X-ray spectra catalyst of LKFeCos700

Table 5.14 Atomic % data of LKFeCos700

LKFeCos700			
S.L.	Element	Weight%	Atomic%
1	O	26.67	39.61
2	Co	4.09	4.76
3	Fe	7.98	2.56
4	K	29.04	21.81
5	La	32.22	31.26
Total		100	100

5.6.1.3 XRD analysis

X-ray diffraction (XRD) studies of the catalysts were carried out to identify the phase and structure of the catalysts. XRD patterns of LKFeCus700-B catalyst compared with the B-site substitution of LKFeCos700 catalysts which is also prepared by the sol-gel method calcinations with temperature 700°C. The detailed X-Ray diffraction

patterns are shown in Figure 5.41. The 2-theta values for LKFeCos700 show that the catalyst has rhombohedral perovskite phase (JCPDS 89-8775). The XRD location peak in XRD patterns of LKFeCus700-B, LKFeCos700 are almost same and showing sharp. Knowing the width of XRD peak and Scherrer equation, the calculated nano-crystalline is presented in Table 5.13. There are no distinct peaks for copper and cobalt in the perovskite catalyst. Therefore it can be confirmed that the mixture is uniform.

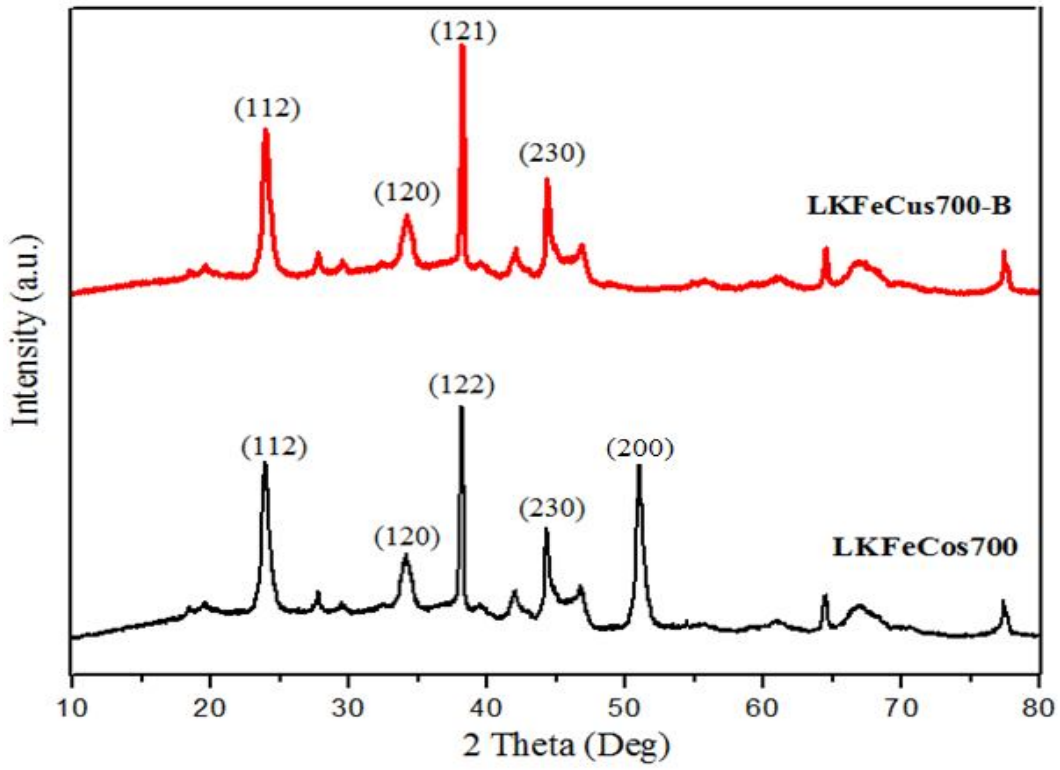

Figure 5.41 XRD comparisons between LKFeCus700-B and LKFeCos700

5.6.2 Catalysts activity tests for simultaneous combustion of soot and reduction of NO

5.6.2.1 Soot combustion

The A-site potassium (K) and B-site cobalt (Co) substitution of $LaFeO_3$ perovskite catalyst (LKFeCos700) was prepared with the same parameter and compared with LKFeCus700-B for simultaneous removal of soot and NO. It was seen from Figure 5.42, LKFeCos700 was showing less soot oxidation activity than LKFeCus700-B

catalyst. The catalytic activity of soot oxidation of T_{10}, T_{50}, $T_{100,}$ and Tp oxidation of diesel soot over the LKFeCos700 catalyst was 147, 221, 403, and 352°C respectively. The catalytic activity of the catalyst samples chiefly depends on three factors: chemical composition, the degree of crystallinity, and the crystals morphology (including particle sizes, pore size distribution, and specific surface area of the perovskite catalyst).

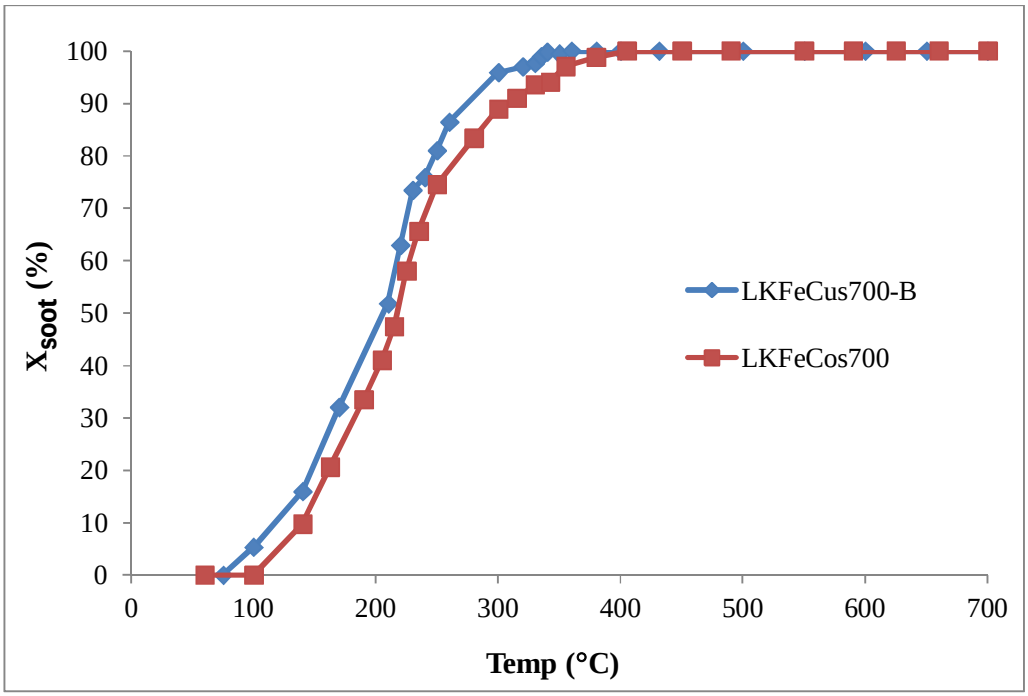

Figure 5.42 Comparative Soot conversion activities between LKFeCus700-B and LKFeCos700

5.6.2.1 NO reduction

The A-site potassium (K) and B-site cobalt (Co) substitution of $LaFeO_3$ perovskite catalyst (LKFeCos700) was prepared with the same parameter and compared with LKFeCus700-B for simultaneous removal of soot and NO. It was seen from Figure 5.43, LKFeCos700 was showing less NO reduction activity than LKFeCus700-B catalyst. The catalytic activity of NO reduction of $T_{max\text{-}NO}$ over the LKFeCos700 catalyst at 366°C was 59.48% which is less than by comparing with LKFeCus700-B.

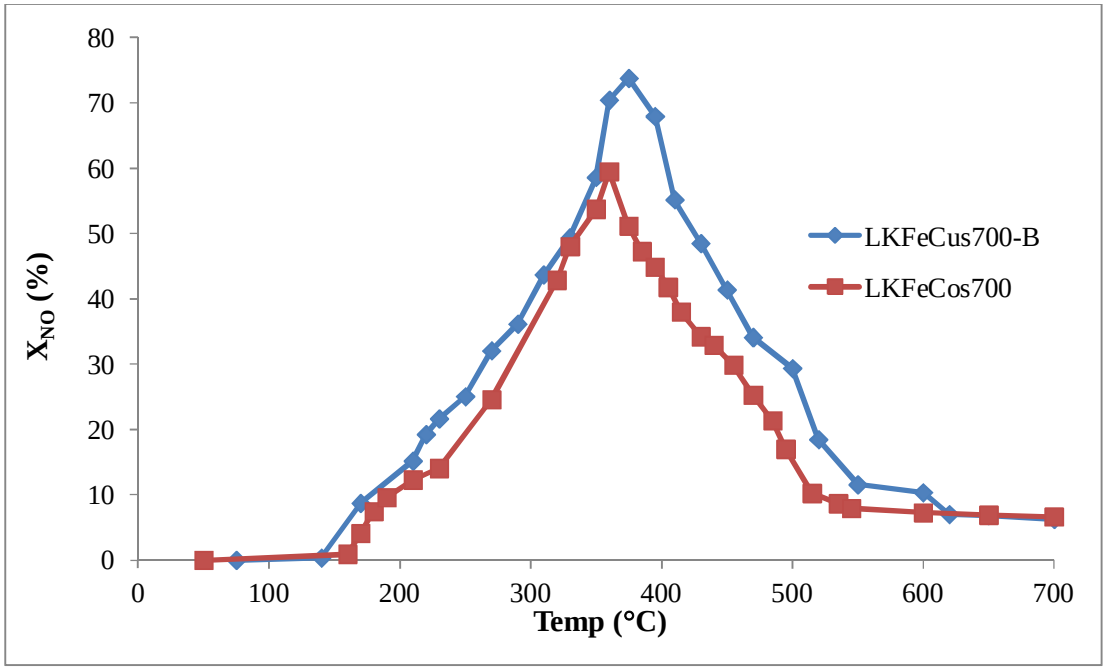

Figure 5.43 Comparative NO conversion activity between LKFeCus700-B and LKFeCos700

5.7 Effect of calcination strategies of the best catalyst

From the experimental data now it is clear that LKFeCus700-B catalyst is the best for simultaneous removal of soot and NO at 369°C. Calcination strategy has great influence on the activity of the catalyst as activity depends on catalyst's physico-chemical properties. The characteristic of catalyst depends on the calcinations atmosphere. Therefore, LKFeCus700-B was subjected to different calcinations atmospheres (stagnant air, flowing air and CO-air mixture) and their activity was checked for simultaneous removal of soot and NO.

5.7.1 Structural and morphological characterization of catalysts

5.7.1.1 Scanning electron microscope (SEM) characterization results

The prepared LKFeCus700-B catalyst was calcined at 700°C in stagnant air, flowing air (FA) and reactive calcination (RC) strategies. The SEM micrographs at 5 KX magnifications shown in Figure 5.44 revealed that the prepared catalyst samples were highly porous and aggregated. The morphologies of particles are irregular shape;

granular particles were also between 40 and 100 nm calculated by "Image J software" with varying degree of agglomeration. In comparison with LKFeCus700-B, LKFeCus700-D, and LKFeCus700-E, the LKFeCus700-E catalyst was more uniform with porous surface.

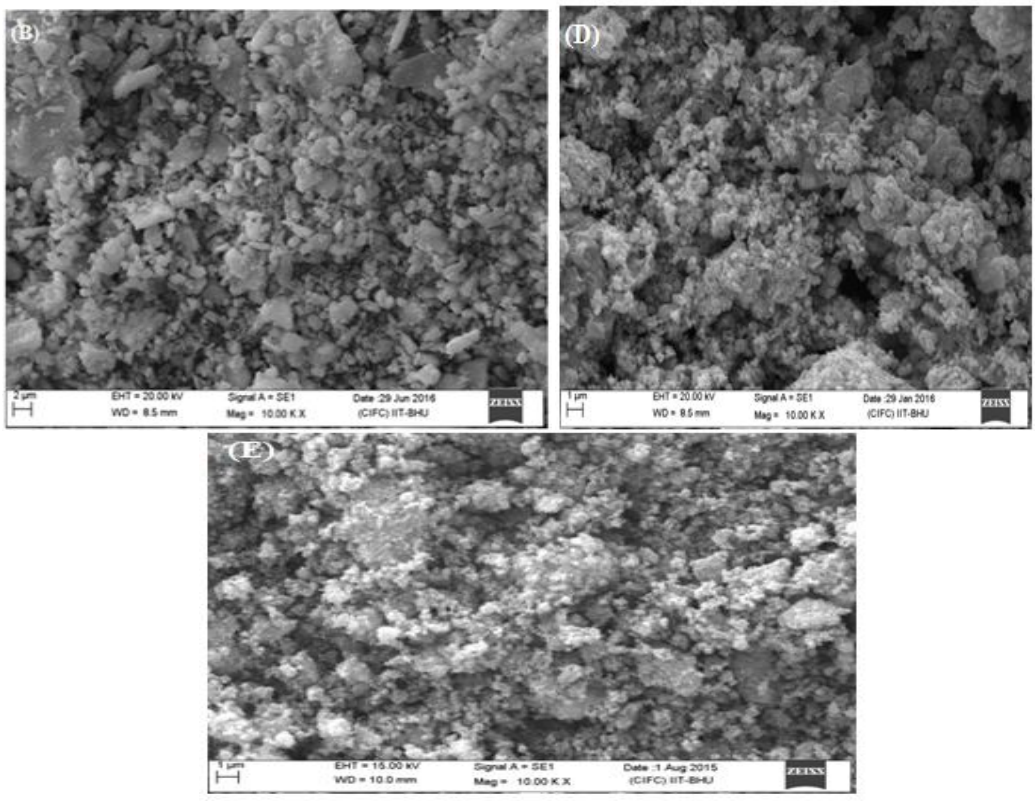

Figure 5.44 Scanning electron micrographs of (B) LKFeCus700-B, (D) LKFeCus700-D, (E) LKFeCus700-E

5.7.1.2 XRD analysis

X-ray diffraction (XRD) studies of the catalysts were carried out to identify the phase and structure of the catalysts. XRD patterns of LKFeCus700-B catalysts compared with flowing air and reactive calcinations condition prepared by sol-gel method and calcinations with temperature 700°C. The detailed X-Ray diffraction patterns are shown in Figure 5.45. The 2-theta values for prepared perovskite show that these catalysts have rhombohedral perovskite phase (JCPDS 89-8775). The XRD location peak in XRD patterns of LKFeCus700-B, LKFeCus700-D, LKFeCus700-E

catalysts showing almost peaks. Knowing the width of XRD peak and Scherrer equation, the calculated nano-crystalline is presented in Table 5.13. All the catalysts showed the similar diffraction pattern.

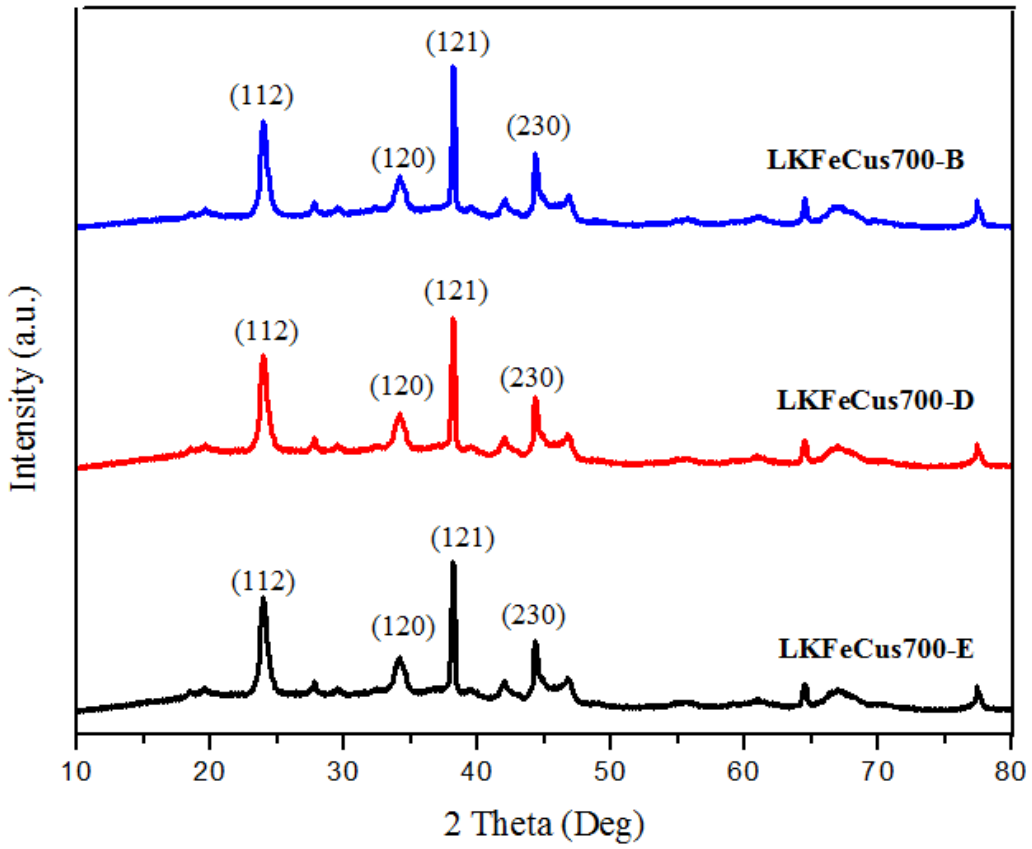

Figure 5.45 XRD of LKFeCus700-A, LKFeCus700-B, LKFeCus700-C

5.7.1.3 Surface area and textural properties of LKFeCus700-E

The LKFCus700-E catalyst calcined at 700°C has highest surface area as compared with catalyst LKFCus700-B, LKFCus700-D calcined at different temperature. The surface area and pore volume follows the trend LKFCus700-E > LKFCus700-D > LKFCus700-B as shown in Figure 5.46 and Table 5.15. The average pore diameter of LKFCus700-B is smallest followed by LKFCus700-D and then LKFCus700-E as shown in Figure 5.47 and Table 5.15.

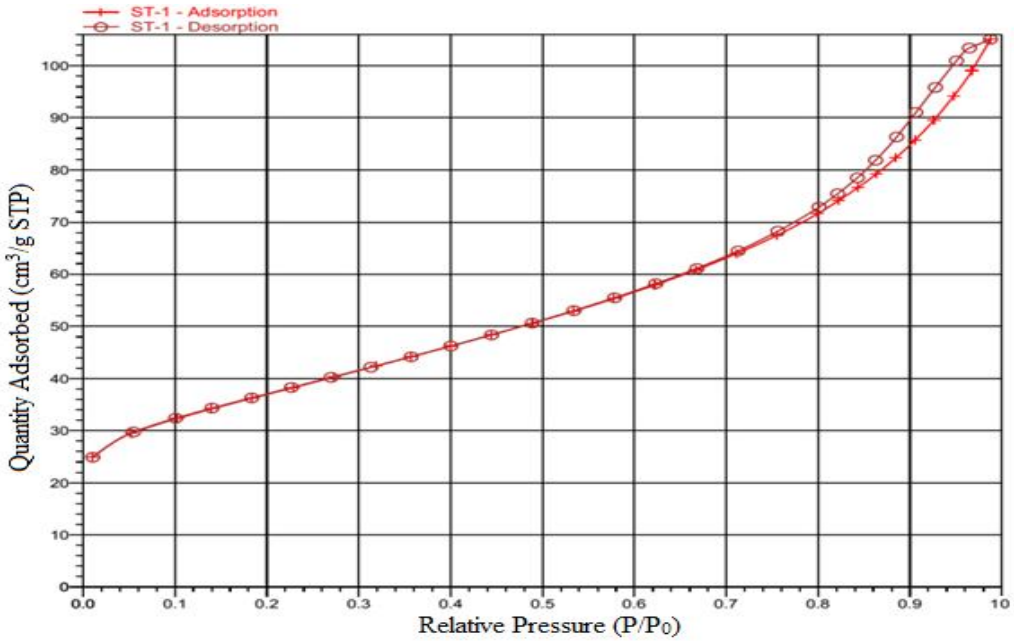

Figure 5.46 Surface area of LKFeCus700-E catalyst

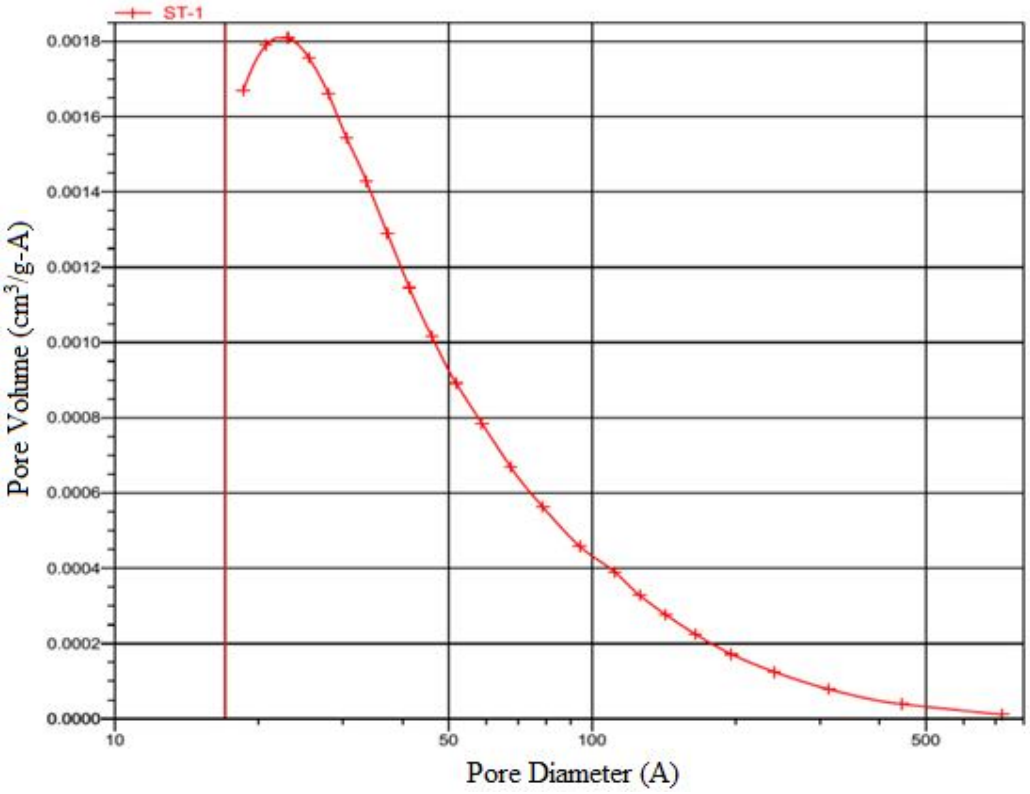

Figure 5.47 Pore volume of LKFeCus700-E catalyst

Table 5.15 Effect of calcination temperature on textural properties of different environment conditions

Catalyst sample	Surface area (m^2/g)	Pore volume (cm^3/g)	Average pore dia. (nm)	Crystallite size (nm)
LKFeCus700-B	23.81	0.0062	27.52	42.57
LKFeCus700-D	22.76	0.0048	28.24	46.34
LKFeCus700-E	**25.11**	**0.0067**	**23.58**	**38.21**

5.7.2 Catalysts activity tests for simultaneous combustion of soot and reduction NO

5.7.2.1 Soot combustion

The prepared LKFeCus700-B catalyst (stagnant air condition) calcined at 700°C by flowing air (FA) and reactive calcination (RC) strategies. The LKFeCus700-D and LKFeCus700-E compared with LKFeCus700-B for simultaneous removal of soot and NO. It was seen from Figure 5.48, LKFeCus700-E was showing high soot oxidation activity than LKFeCus700-B and LKFeCus700-D catalysts. The catalytic activity of soot oxidation of T_{10}, T_{50}, $T_{100,}$ and Tp oxidation of diesel soot over the LKFeCus700-E catalyst was 123, 206, 347, and 309°C respectively. The catalytic activity of the catalyst samples chiefly depends on three factors: chemical composition, the degree of crystallinity, and the crystals morphology (including particle sizes, pore size distribution, and specific surface area of the perovskite catalyst).

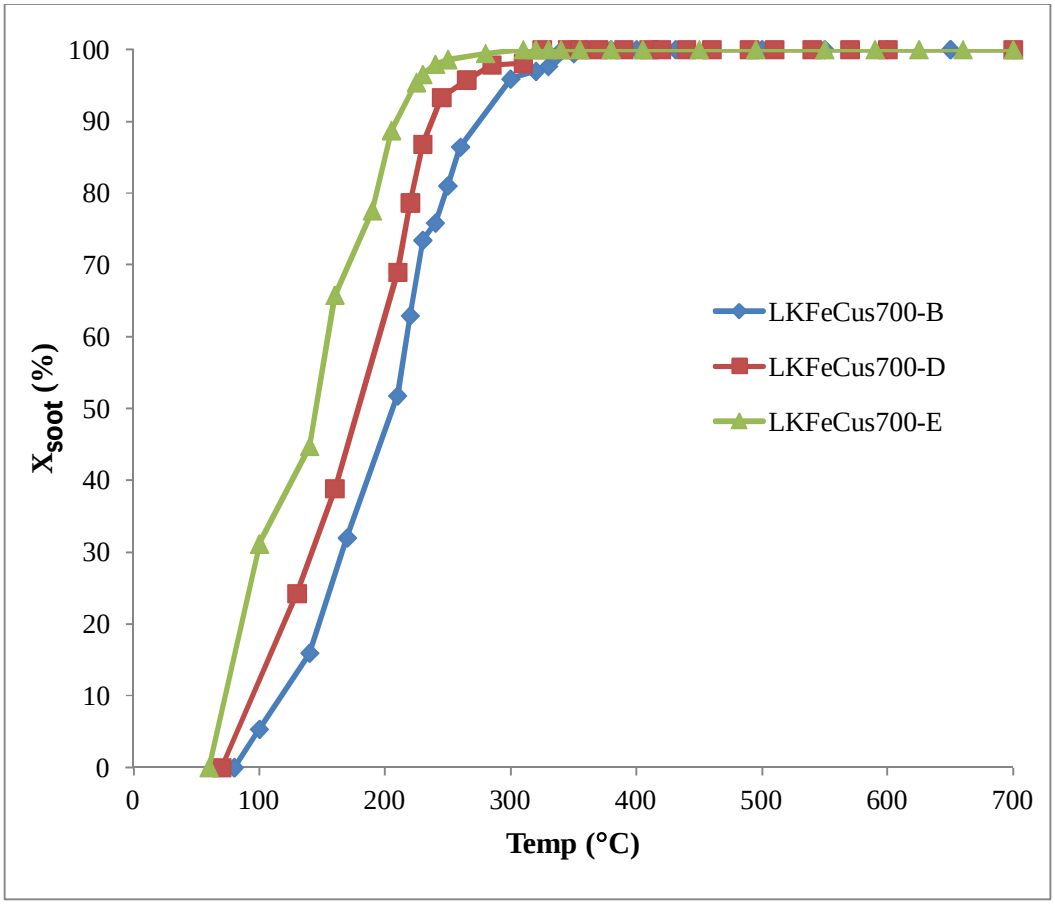

Figure 5.48 Soot conversion activities by different calcinations strategy

5.7.2.2 NO reduction

The prepared LKFeCus700-B catalyst (stagnant air condition) calcined at 700°C by flowing air (FA) and reactive calcination (RC) strategies. The LKFeCus700-D and LKFeCus700-E compared with LKFeCus700-B for simultaneous removal of soot and NO. It was seen from Figure 5.49, LKFeCus700-E was showing more NO reduction activity than LKFeCus700-B and LKFeCus700-D catalysts. The catalytic activity of NO reduction of $T_{max\text{-}NO}$ over the LKFeCus700-E catalyst was at 361°C was 75.62%.

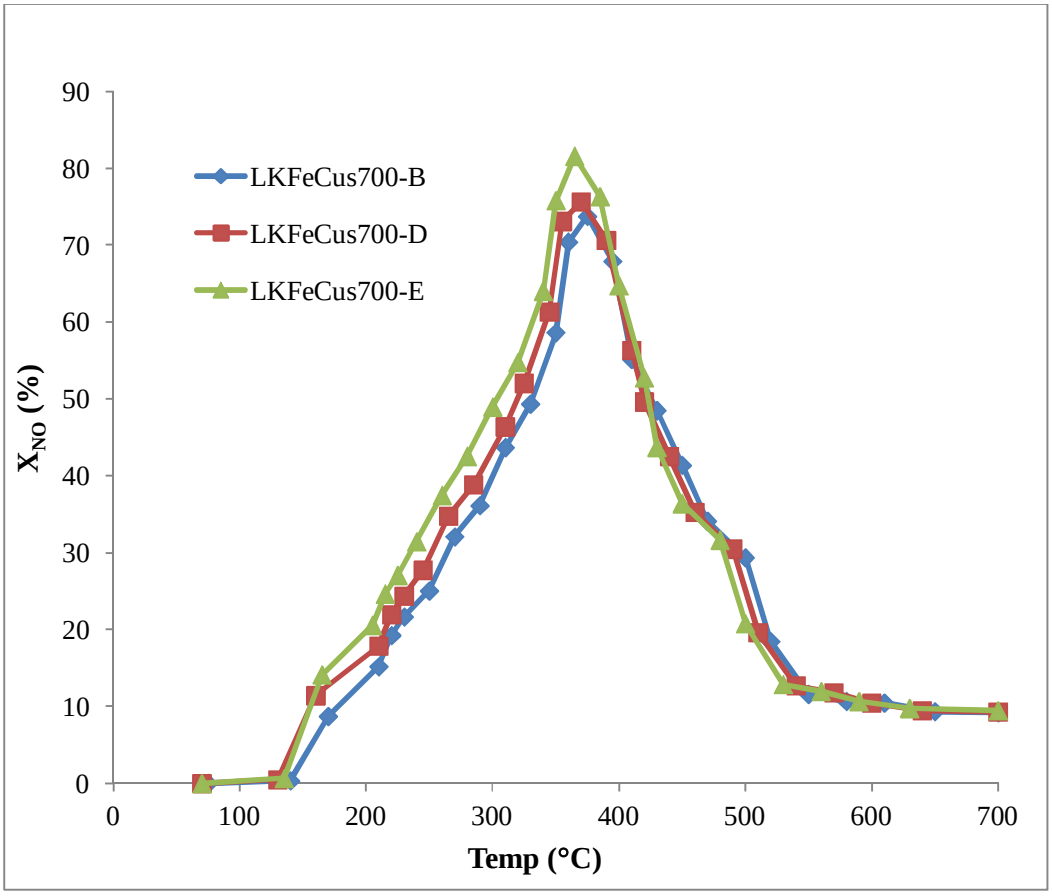

Figure 5.49 Soot conversion activities by different calcinations strategy

5.8 Comparison of soot conversion activity under loose and tight contacts

The comparison between tight and loose contact condition of pure $LaFeO_3$ (Figure 5.50), LKFeCus700-B (Figure 5.51), LKFeCus700-E (Figure 5.52) catalysts with soot, the soot conversion activity of tight contact was more high due to the proper mixing and higher external surface area. It is a clear correlation of the decrease in the soot oxidation temperature with the increase in the surface area of the catalyst by spreading the soot properly on the catalyst surface. The higher external surface areas have the superior oxidation performance.

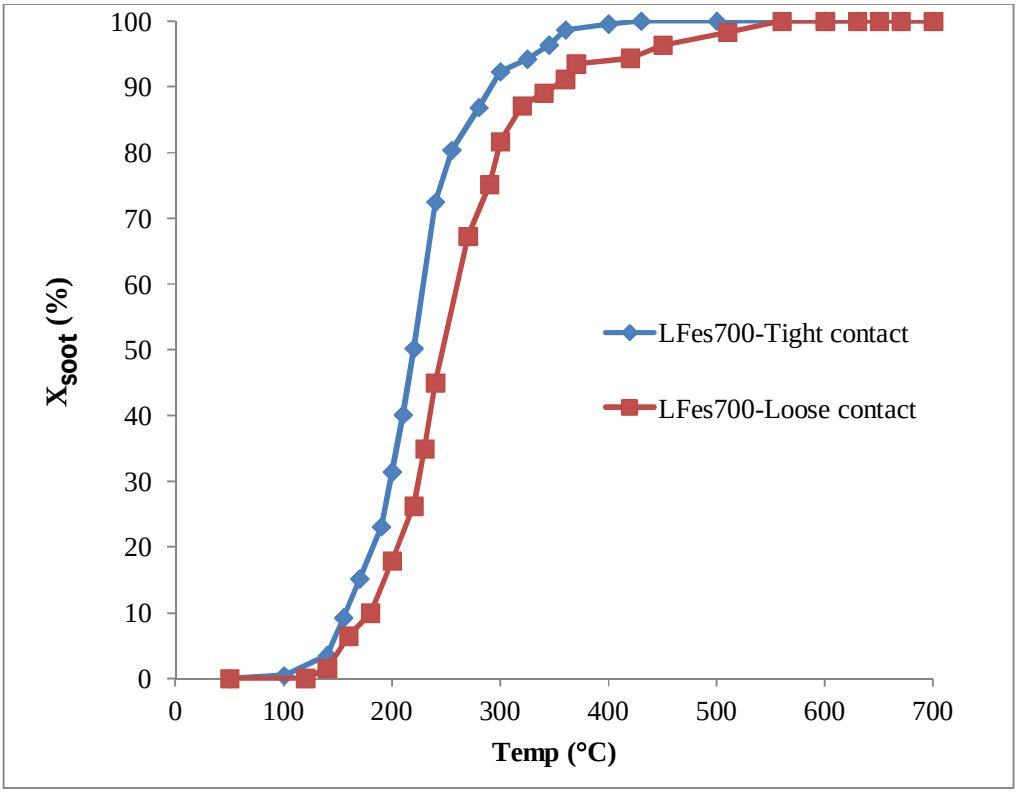

Figure 5.50 Effect of contact type on soot oxidation on LFes700 catalyst (1000 ppm NO, 10% O_2+ 99.9% Ar)

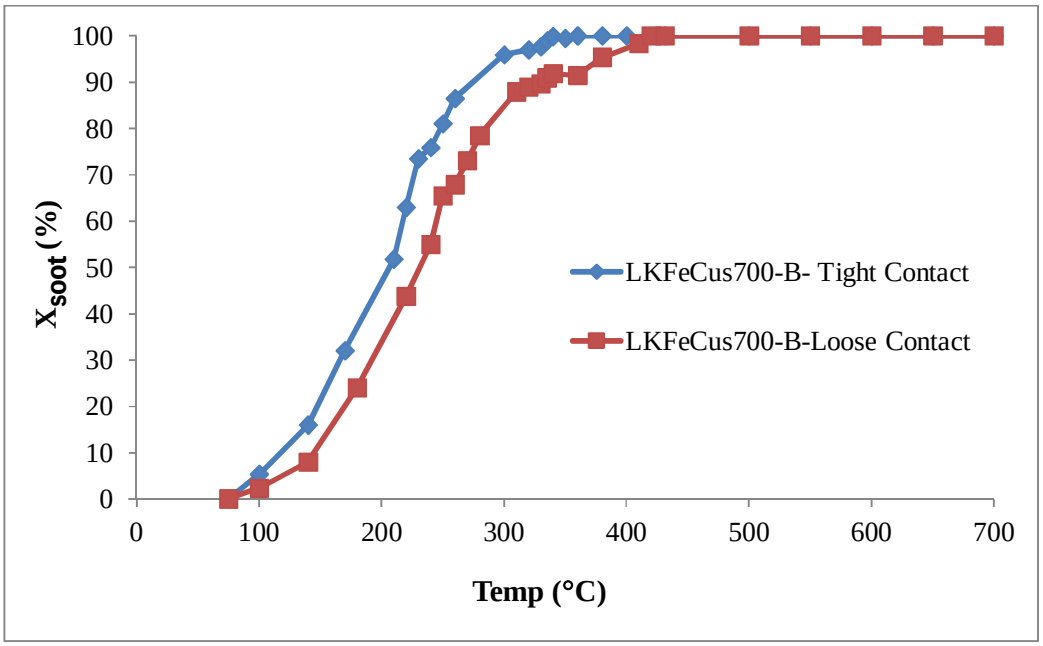

Figure 5.51 Effect of contact type on soot oxidation on LKFeCus-B catalyst (1000 ppm NO, 10% O_2+ 99.9% Ar)

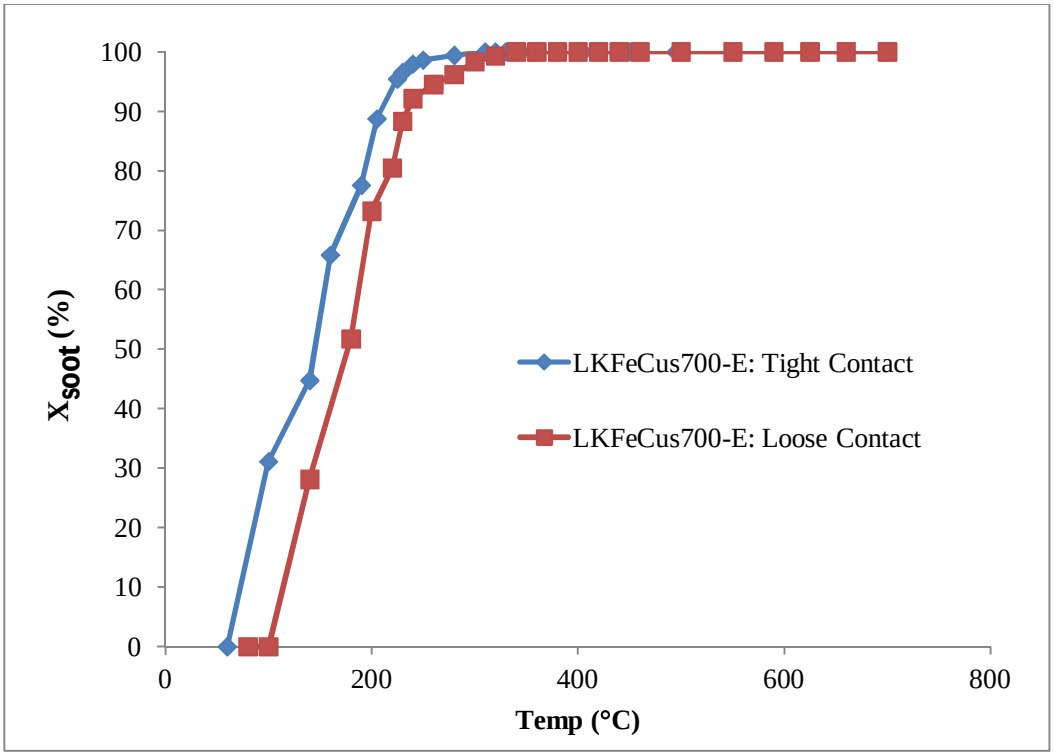

Figure 5.52 Effect of contact type on soot oxidation on LKFeCus-E catalyst (1000 ppm NO, 10% O_2+ 99.9% Ar)

5.9 Comparison of soot conversion activity without NO

The soot conversion activities were examined for LFes700, LKFes700, and LKFeCus700-B (Figure 5.53) absent of NO. It was seen that less oxidizing activity of all catalysts in absent absence of NO because NO worked as an oxidizing agent for soot oxidation. The NO conversion to NO_2 over these catalysts is responsible for higher the soot oxidation activity. NO_2 concentration reaches the maximum value when the soot is burned completely. Because NO_2 is a more powerful oxidant than O_2 for soot oxidation, leading to the NO conversion to NO_2 efficiently decrease the soot combustion temperature. It implies the consumption of NO_2 by reaction with soot at low temperatures which form the surface oxygenated species C(O). Afterwards, the C(O) can either be decomposed to release CO or be oxidized by O_2 to produce CO_2. When the soot reaction is finished, the main production is NO_2.

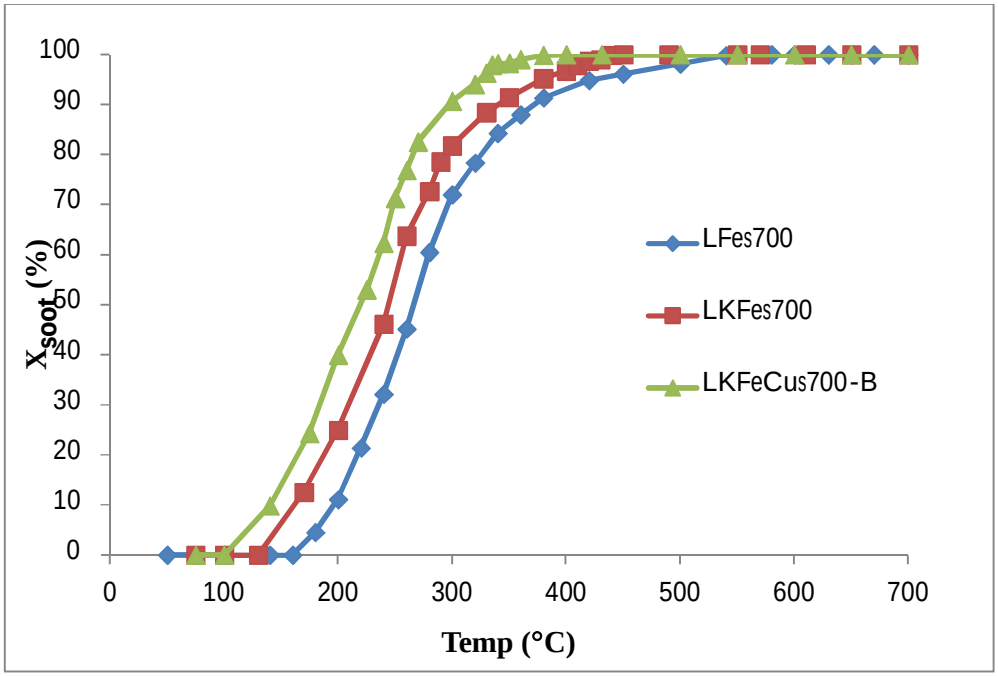

Figure 5.53 Effect of soot conversion over perovskite-type catalysts without NO (calcined at 700°C, Catalyst / Soot: 10/1, tight Contact, flow rate: 100 ml/min)

5.10 Comparison of NO conversion activity under loose and tight contact conditions

The comparison between tight and loose contact condition of pure $LaFeO_3$ (Figure 5.54), LKFeCus700-B (Figure 5.55), and LKFeCus700-E (Figure 5.56) catalysts with soot, the NO conversion activity of tight contact was less due to the calcination of the catalyst. It is a clear correlation of the increase in the NO reduction temperature with the increase in the surface area of catalyst by spreading the soot tightly on the catalyst surface. Under tight contact soot cover higher fraction of catalyst surface area while, loose contact has relatively lower fraction of catalyst surface covered by soot. So a favorable fraction of the surface is available for both soot and NO to react each other over the catalyst under loose contact, resulting higher conversion than tight contact.

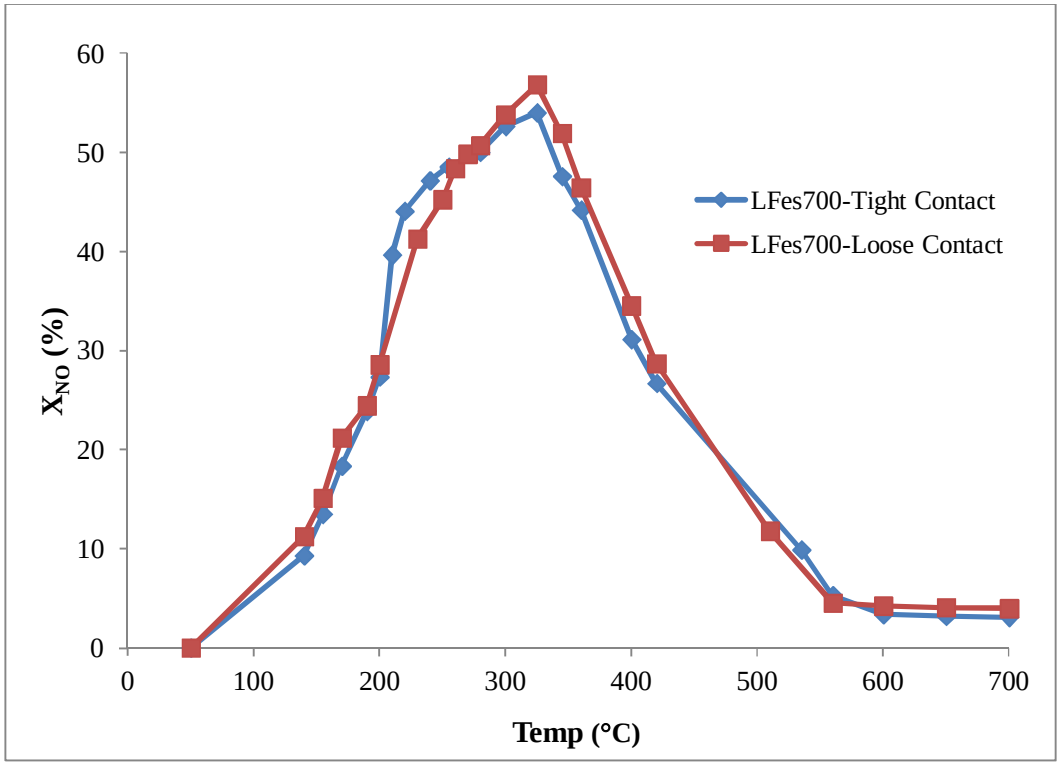

Figure 5.54 Effect of NO conversion activity different contact condition on LFes700 catalyst (1000 ppm NO, 10% O_2+ 99.9% Ar)

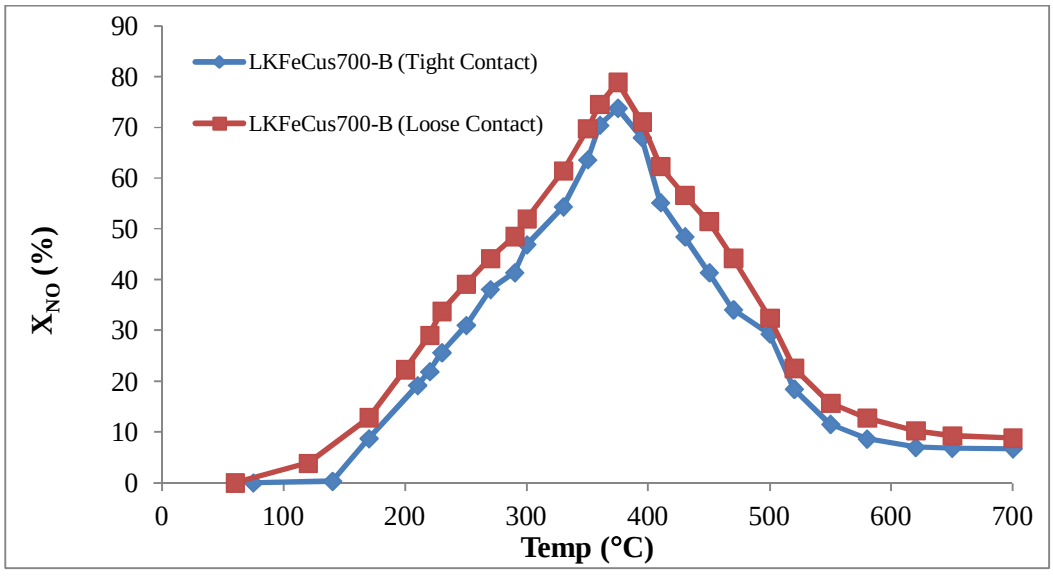

Figure 5.55 Effect of NO conversion activity different contact condition on LKFeCus700-B catalyst (1000 ppm NO, 10% O_2 + 99.9% Ar)

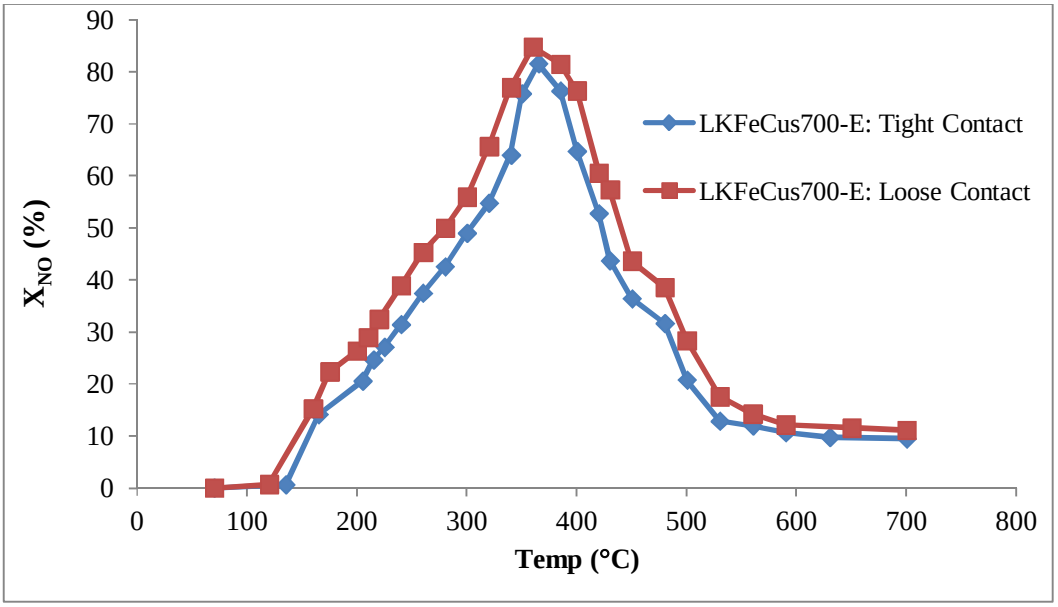

Figure 5.56 Effect of NO conversion activity different contact condition on LKFeCus700-E catalyst (1000 ppm NO, 10% O_2 + 99.9% Ar)

5.11 NO decomposition over catalyst

Direct decompositions of nitric oxide by LFes700, LKFes700, and LKFeCus700-B are experimentally investigated at various temperatures (150-600°C) as shown in Figure 5.57. Experimental results indicate that the physical and chemical properties of $LaFeO_3$ are significantly improved by partial A-site K and B-site Cu substitutions, the NO decomposition efficiencies achieved with LKFeCus700-B is nearly 5% at 600°C. It is expected that the properties and activities of the catalysts can be improved to further reduce the reaction temperature needed for NO decomposition. Influences of space velocity, O_2, H_2O (g), and CO_2 on NO decomposition are also evaluated with a laboratory-scale experimental system.

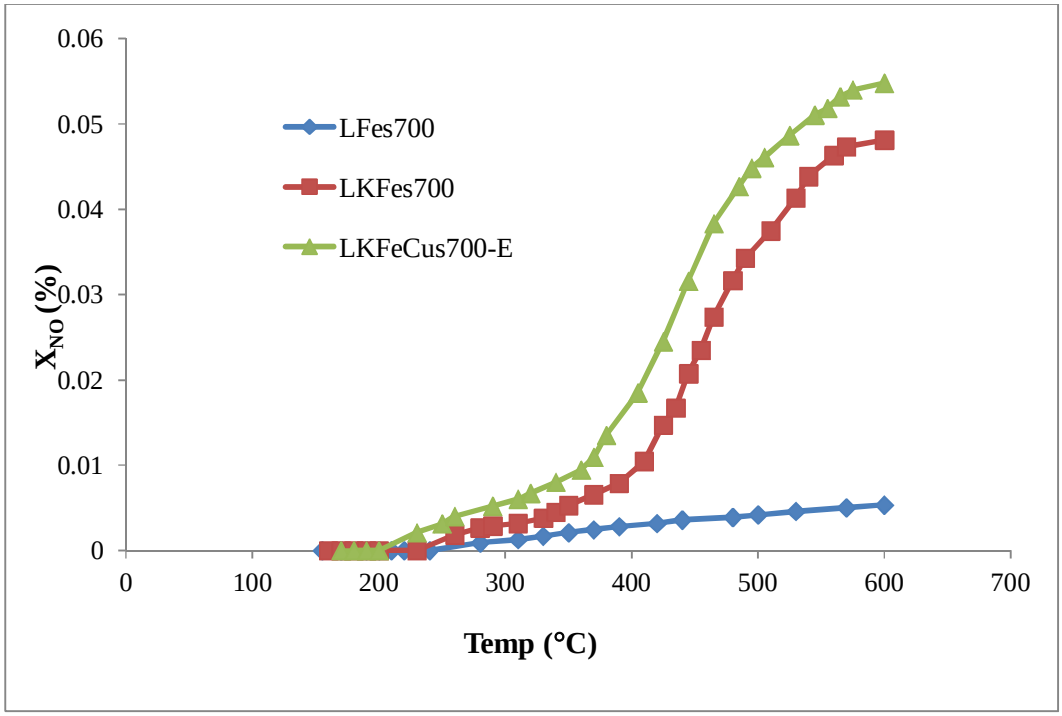

Figure 5.57 NO decomposition at different temperatures

5.12 Stability Test of the Best Catalyst

The time on stream stability test of LKFeCus700-E catalyst was conducted at 350^{o}C for simultaneous removal of soot and NO in a continuous running for 50h under the earliest mentioned experimental conditions. It can be seen in the Figure 5.58 that at 350^{o}C, 100% soot conversion and 75.81% NO conversion were maintained for 50hrs. The result revealed that practically no deactivation of the LKFeCus700-E catalyst has occurred in the experimental conditions. It was confirmed that the LKFeCus700-E catalyst is stable for 50h under continue running process. The extraordinary performance of LKFeCus700-E catalyst produced by RC for simultaneous removal of soot and NO was associated with the modification in intrinsic textural, morphological characteristics such as surface area, crystallite size and particle size of the catalyst. The performance of the catalyst was judged by their activity, selectivity, and stability.

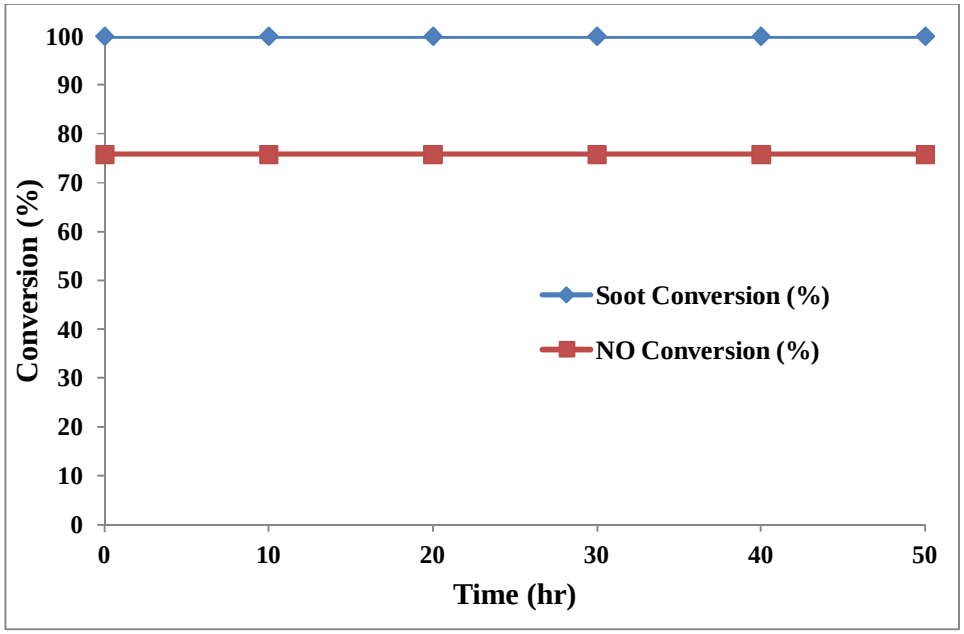

Figure 5.58 Time on stream stability test of LKFeCus700-E catalyst for simultaneous removal of soot and NO

5.13 Selectivity of the Best Catalyst

The selectivity test of LKFeCus700-E catalyst was conducted for simultaneous removal of soot and NO in the bench scale reactor as earlier mentioned experimental conditions. There was no CO detected in the influent stream, thus catalyst was 100% selective towards CO_2. The selectivity for N_2 and N_2O are shown in Figure 5.59. It can be seen from the figure that selectivity curve for N_2 shows a minimum value of 94% at 250°C. Beyond 250°C selectivity, S_{N2} increases and reach 100% at 300°C. Beyond 300°C S_{N2} becomes >100%, this is because N_2 is formed by soot oxidation as well as by NO decomposition thermally over the catalyst without soot as shown in Figure 5.57. Whereas, N_2O selectivity curve shows maximum value of 8% at 300°C. Beyond 300°C the selectivity decreases to a minimum value 4% above 400°C. Therefore the catalyst maintained the good selectivity.

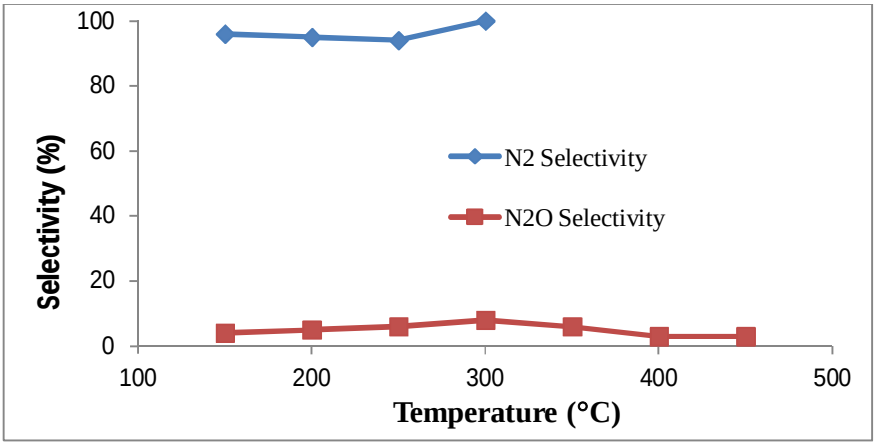

Figure 5.59. Selectivity to N_2 formation (S_{N2}) and N_2O formation (S_{N2O}) LKFeCus700-E catalyst

Table 5.16 Overall activities of prepared catalysts

S. L.	Catalyst	Soot oxidation				NO reduction	
		T_{10} (°C)	T_{50} (°C)	T_{100} (°C)	T_p (°C)	T_{max} (°C)	X_{NO} (%)
1	LFes600	217	322	482	441	384	47.31
2	LFes650	196	290	514	365	319	49
3	LFes700	168	218	429	323	325	54
4	LFes750	181	267	436	422	372	51.05
5	LFesc700	236	283	451	344	335	46.91
6	LFerg700	288	301	466	361	342	43.45
7	LCos700	273	372	489	428	374	51
8	LMns700	215	324	482	369	349	48.61
9	LKFes700	124	213	407	339	340	59.29
10	LKFeCus700-A	161	269	438	351	393	63.73
11	LKFeCus700-B	133	207	363	326	369	71.41
12	LKFeCus700-C	141	234	377	343	384	67.59
13	LKFeCos700	147	221	403	352	376	59.48
14	LKFeCus700-D	128	206	356	317	364	72.58
15	LKFeCus700-E	123	202	347	309	361	75.62

Based on the experimental results and discussion following conclusions can be drawn:

i. The literature review reported in the thesis includes the investigation carried out on the simultaneous catalytic control of diesel soot and NOx till date.

ii. Perovskite catalysts are active and cost-effective for simultaneous soot-NOx reduction and are emerging as an alternative to the PGM catalysts.

iii. Substituted perovskite structured catalysts are more active than other type of catalysts for the simultaneous soot-NOx reaction.

iv. Potassium substitution at A-site of $LaFeO_3$ catalyst improves the catalytic activity for simultaneous soot-NOx reduction.

v. The high activity of LKFes700 perovskite catalyst is attributed to the presence of metallic potassium in the catalyst.

vi. Double substitution of Potassium substitution at A-site and Copper substitution at B- site of $LaFeO_3$ catalyst improves the catalytic activity for simultaneous soot-NOx reduction.

vii. The activity order of K and Cu doped $LaFeO_3$ is as follows

LKFeCus700-B > LKFeCus700-C > LKFeCus700-A

viii. The strategies of the catalyst by reactive calculation LKFeCus700-E and flowing air LKFeCus700-D, stagnant air of LKFeCus700-B examined, the reactive calcinations (of LKFeCus700-E) catalyst was showing more catalytic activity for simultaneous soot-NOx reduction.